Supplementary Materials for

Transition from global stability to multiple attractors in microcosms

This PDF file includes:

Methods
Supplementary Figs. 1 to 38

Methods

Bacterial isolates, media and culturing conditions

We constructed the library of 54 bacterial species using isolates from soil samples. This library is phylogenetically diverse, with isolates coming from 4 different phylums: Proteobacteria, Firmicutes, Bacteroidota and Actinobacteriota.

In the case of low interaction strength (low nutrients concentration) conditions, experimental communities were cultured in Base Medium (BM): 1gL^{-1} yeast extract and 1 gL^{-1} soytone from Becton Dickinson, 10 mM sodium phosphate, 0.1 mM $CaCl_2$, 2 mM $MgCl_2$, 4mgL^{-1} $NiSO_4$ and 50 mgL^{-1} $MnCl_2$, pH adjusted to 6.5. For the high interaction strength (high nutrients concentration) condition, we used BM supplemented with 20 gL^{-1} glucose and 16 gL^{-1} urea. The strong pH buffer media is the high nutrient media (normal buffer) with extra added sodium phosphate (pH buffer): 100 mM sodium phosphate, 20 gL^{-1} glucose, 16 gL^{-1} urea, 1gL^{-1} yeast extract, 1 gL^{-1} soytone, 0.1 mM $CaCl_2$, 2 mM $MgCl_2$, 4mgL^{-1} $NiSO_4$, 50 mgL^{-1} $MnCl_2$, pH adjusted to 6.5.

All media were filter sterilized using Bottle Top Filtration Units (VWR). All of the chemicals were purchased from Sigma–Aldrich unless otherwise stated. Both monocultures and communities of the bacterial isolates were grown in 96-deepwell plates (Deepwell plate 96/1000µl; Eppendorf) covered with AeraSeal adhesive sealing films (Excel Scientific). The incubation temperature was 30 °C for all communities. The deepwell plates were shaken at 900 r.p.m. on Titramax shakers (Heidolph).

Community assembly experiment protocol

Prior to the community assembly experiments, each of the 54 isolated bacterial strains was first cultured individually in 300 µL of Base Medium and allowed to grow under stable conditions for approximately 24 hours. To construct the initial communities composed of S species ($S = 6,12,24$), we systematically prepared many (usually 8, at least 6, at most 32) distinct initial species compositions through a multi-step dilution and mixing process. Specifically, equal volumes of the pre-grown monocultures were thoroughly mixed, and this homogenized mixture was diluted in sterile phosphate-buffered saline (PBS) to achieve a 100-fold dilution. Subsequently, 10 µL of this diluted suspension were separately combined with 10 µL of each of the eight dominant species' undiluted cultures to get widely different initial species abundances, each with 1:99 species ratio. These preparations were then subjected to an additional 100-fold dilution in sterile PBS, after which 30 µL of the diluted suspensions were inoculated into 300 µL of fresh culture medium. This procedure generated 8 replicate communities with precisely controlled initial species abundance profiles, which were subsequently incubated at 30°C for 24 hours to initiate growth.

Daily dilutions with controlled dispersal

For each microbial community, we performed seven 24-hour transfer cycles combining dilution and dispersal. For most of our assembled communities with dilution rate 1000, each cycle began with a 1000-fold dilution of the community, followed by addition of a dispersal inoculum (a 200,000-fold diluted, uniformly mixed suspension of all species). For the communities with dilution rate 100,000, each cycle began with a 100,000-fold dilution of the community, with similar following protocols. All liquid handling was automated using a 96-channel electronic pipette (Viaflo 96, Integra

Biosciences). Each mixing process in 200μL medium is operated by Viaflo 96 with five 100μL pipette/mix cycles), and in 300μL medium is operated by Viaflo 96 with 150μL pipette/mix cycles.

Biomass and pH measurements

The total biomass of the microbial communities was measured using a Tecan microplate reader. At each growth cycle, 100 μL of homogenized culture was transferred to a flat bottom Falcon® 96-well Clear Microplate, and the optical density (OD 600nm) was measured to assess culture turbidity, which correlates linearly with total biomass within a specific range. Blank controls containing an equal volume of sterile PBS were included for baseline calibration. For pH measurement, the community pH was determined using a Thermo Scientific Orion Star A211 benchtop pH meter. At the end of the seventh transfer cycle, 100 μL of homogenized culture was aliquoted into a 96-well PCR plate, and the pH of each community was measured sequentially.

DNA extraction and 16S rRNA sequencing and data analysis

To monitor the dynamics of the microbial communities, we measured community composition via 16S ribosomal RNA (rRNA) amplicon sequencing. For community time series profiling, representative communities were sampled across seven daily cycles, while the remaining communities were sample at the seventh cycle for steady-state characterization. The DNA extraction was performed with the Zymo Research Quick-DNA Fungal/Bacterial 96 Kit following the protocol provided by the manufacturer. The extracted DNA was used for 16S rRNA gene amplicon sequencing targeting the V4–V5 region. Library preparation and Illumina sequencing (NovaSeq Reagent Kit, 500 cycles) were performed by Novogene. Sequencing covered the V4–V5 region, generating 250 bp reads in both the forward and reverse directions. We used the R package DADA2 to obtain the amplicon sequence variants (ASVs) as described by Callahan et al. Taxonomic identities were assigned to the ASVs by using SILVA (version 138) as a reference database. To address intragenomic 16S rRNA variation, we merged correlated ASVs ($r>0.99$, co-occurring in all cultures with identical ratio) into combined ASVs representing single species.

Based on the ASV reads number for each bacterial isolate culture, we classified the 54 bacterial isolates into distinct species based on the similarity of their genomic abundance profiles. Isolate pairs showing near-identical abundance patterns (Pearson correlation > 0.95) were considered to belong to the same species. This approach identified 33 distinct species among the isolates, with their genus-level distribution shown in Fig. S3. Phylogenetic tree analysis was performed using MAFFT for sequence alignment, IQ-TREE for maximum-likelihood tree construction, and iTOL for visualization.

Based on the ASV-isolate mapping, we analyzed species abundance profiles across all assembled communities. To minimize noise from non-target taxa, we focused on abundances of ASVs corresponding exclusively to each community's predefined species pool, which aligned closely with raw compositional data in most cases. Discrepant communities showing large differences between raw and ideal abundances were retained in raw data. The species relative abundance is calculated by the ASV reads number normalized to sum to 1 per sample. The absolute abundance is normalized by the total community biomass (OD).

Numerical methods

We modeled the long-term dynamics of ecological communities using the well-known generalized Lotka-Volterra (gLV) model, modified to include dispersal from a species pool:

$$\frac{dN_i}{dt} = r_i N_i \cdot \left(1 - \sum_{j=1}^{S} \alpha_{ij} N_j\right) + D \qquad i = 1,2,\dots,S$$

where N_i is the abundance of species *i* (normalized to its carrying capacity), α_{ij} is the interaction strength that captures how strongly species *j* inhibits species *i* (with self- regulation α_{ii} = 1), and *D* is the dispersal rate of each of the *S* species. For simplicity and without qualitatively changing our results, we considered the same growth rate $r_i = 1$ and the same carrying capacity $K_i = 1$ for all species. All simulations used the 4th-order Runge-Kutta (RK4) method on Matlab to numerically solve the gLV equations (with an integration step of 0.1). The total simulation time is set to be 1500 to guarantee that the stable community have reached steady states.

Definition of stable and fluctuating dynamics *in silico*

To differentiate between stable and fluctuating communities, we computed the maximum coefficient of variation of N_i between *t*=1400 and *t*=1500, corresponding to species abundances during the final 1000 steps. We define communities with this average coefficient of variation higher (lower) than 10^{-3} as fluctuating (stable) communities.

Definition of multistability *in silico*

For each community, we simulated many different initial species abundances until they reached steady state. Since the simulation time is long enough for most of the communities to be steady, we took the endpoint representing the potential stable states. For all the stable replicates in a single community, we classified replicate communities as belonging to the same stable state when the maximum absolute difference in all species abundances was below a strict threshold. The threshold is set to be 0.05, and it is robustly effective in the range $[10^{-3}, 10^{-1}]$. Specifically, two replicates 1 and 2 were considered compositionally identical if:

$$\max_i |N_{i,1} - N_{i,2}| < threshold$$

where $N_{i,1}$ and $N_{i,2}$ represent the abundance of species i for replicates 1 and 2, $i = 1,2,\dots,S$. This criterion was applied iteratively to establish new state profiles from unclassified replicates and assign subsequent replicates to existing states when all species-wise differences satisfied the threshold condition. If the community's stable replicates exhibit more than one stable state, the community is classified as having multiple stable states. If the community exhibit only one stable state and without fluctuating dynamics in every replicate, it is classified as globally stable community.

Definition of multiple attractors *in silico*

Communities can reach different dynamical attractors if given different initial species abundances. A community is classified as having multiple attractors, if different species abundances can lead to at least two different stable or fluctuating attractors—identified by the criteria of stability and multistability. Here, all fluctuating states in a fixed community were treated collectively as one fluctuating state in our analysis. Notably, it is possible to distinguish between distinct fluctuating

attractors by comparing species composition and abundances during a period of time (such as during the final 1000 steps), since the time variance has been diminished. However, since it is inherently challenging to rigorously distinguish between fluctuating dynamics and is also hard to correlate with the experiment, we did not attempt to further subclassify these dynamic regimes.

Theoretical prediction for the stability phase diagram

The analytical boundary between the stable phase (II) and unstable phase (III) was derived in Bunin 2017. For equal carrying capacities, it is shown that the boundary lies at the average standing species richness $S^* = S/2$, when $\sigma \equiv \sqrt{S}\, std(\alpha_{ij})/(1 - \langle \alpha_{ij} \rangle) = \sqrt{2}$.

Simulation of phase diagram

To test the transition from stable phase to multiple attractors, we employed numerical simulations to systematically examine how two key ecological parameters shape the dynamic stability of microbial communities: (1) the average species interaction strength ($< \alpha_{ij} >$) and (2) the size of the species pool (S). A definition of 20 × 20 or 30 × 30 pixels was used for each phase diagram, linearly segmenting the parameter space in the ranges $< \alpha_{ij} > \in [0, 1]$ and $S \in [1, 60]$ or even larger. In each phase diagram, each pixel shows the average result for 256 different communities with randomly sampled interaction matrix. For each community with species pool size S and interaction strength $< \alpha_{ij} >$, we tested 100 initial species abundances, including conditions where one species dominated ($N_i = 0.1$) while the others had small initial abundances ($N_j = 10^{-4}$), as well as conditions where the initial abundances of each species were randomly drawn from a uniform distribution spanning [0,1].These different initial abundances led to different outcomes of community assembly: some community converged to a globally stable equilibrium where all initial abundances reached the same final state, while others produced persistent fluctuations or alternative states. Communities with alternative states could exhibit multistability or multiple dynamical attractors that include both stable and fluctuating dynamics (Figure S1).

In these simulations, globally stable communities refer to the communities that all our tested initial abundances converge to a single stable state. Multi-stable communities refer to the communities with multiple stable states, regardless of whether it could fluctuate under some initial species abundances. Pure multi-stable communities refer to the communities exhibiting multiple stable states and without persistent fluctuating dynamics in all our tested initial conditions. Fluctuation communities refer to the communities that could go to fluctuation under certain initial species abundances. Pure fluctuation communities refer to the communities that fluctuate in all our tested initial species abundances and showing no stable states. Fluc-stable communities refer to the communities that could either converge to stable state or fluctuate depending on initial species abundances. Multi-attractor communities refer to the communities with multiple dynamical attractors, such as multiple stable states or having both stable and fluctuating states.

Definition of stable and fluctuating experimental communities

We classified communities as either stable or fluctuating based on temporal biomass variability during the final experimental period (days 5–7). For each replicate community, we calculated the standard deviation (σ) of its optical density (OD) measurements across this 3-day window. Communities were designated as either stable ($\sigma \leq 0.15$) or fluctuating ($\sigma > 0.15$). For the

communities with all the replicate being stable, we further analyzed the stable states number and whether it exhibits global stability, functional bistability, compositional multistability or hybrid multistability.

Quantification of stable states number in experiment

To determine the number of stable states for each community, we performed hierarchical clustering (average linkage method) on the absolute abundance profiles of eight replicate samples at steady state, using Bray-Curtis dissimilarity as the distance metric. A conservative clustering threshold was applied to account for technical variations (e.g., sequencing errors and replicate variability). The number of clusters identified at this threshold represented the observed multiplicity of stable states for a given community. In the main text, we set the threshold to be 0.45. We also tested higher or lower threshold in supplementary figures.

The Bray-Curtis dissimilarity—a widely adopted β-diversity measure in microbial ecology—quantifies compositional differences between samples while being independent of total abundance. It is defined as:

$$BC\ distance = 1 - \frac{\sum_i min(N_{i1}, N_{i2})}{(\sum_i N_{i1} + \sum_i N_{i2})/2}$$

where N_{i1} and N_{i2} represent the abundance of species i in Sample 1 and Sample 2, respectively. The index ranges from 0 to 1, where 0 represents complete compositional overlap and identical species abundances, 1 represents no shared species and completely distinct communities.

Classification of four community types in experiment

To quantitatively classify the four stability types, we established a two-step classification system based on biomass variation and compositional dissimilarity. First, communities were categorized as functionally bistable if their maximum biomass difference (OD) among replicates exceeded 0.5, otherwise they were classified as having a single functional state. Second, compositional multistability was determined by calculating the maximum Bray-Curtis dissimilarity of species absolute abundances (derived from sequencing data and biomass measurements) within one functional regime: for functionally uniform communities, we used all pairwise comparisons between replicates, while for functionally bistable communities we separately analyzed high- and low-biomass groups and then selected the larger maximum dissimilarity value. Applying a universal compositional threshold of 0.45, communities were further classified as compositionally multistable or hybrid multistable if dissimilarity ≥0.45, and globally stable or functionally bistable if dissimilarity <0.45.

We also tested Bray-Curtis dissimilarity of species relative abundances (threshold 0.4) and other normalized dissimilarity metrics, such as correlation distance of absolute abundances (threshold 0.25), the classification remains robust. Moreover, the classification scheme proved robust across different dilution factors, demonstrating its reliability for characterizing microbial community stability patterns.

The introduction of eLV (environment-coupled Lotka-Volterra) model

To explicitly integrate low-dimensional global environmental coupling together with the

intrinsically high-dimensional interspecies interaction network, we developed an environment-coupled Lotka-Volterra (eLV) model (Figure S29). This model incorporates a global environmental variable and associated dynamical equation the classical gLV model that has one equation for each of the *S* species. The global environmental variable is meant to capture the dominant way in which species interact through their shared environment (in this case the pH, although other environmental variables such as oxygen availability may have similar dynamics). We assume that the global environmental variable *e* can be modified by species in the community and modifies the growth rate of each species. Finally, the global environmental variable exhibits self-regulation, relaxing toward equilibrium at a rate δ, with typical variation set by linear and cubic restoring terms. The self-regulation corresponds to the tendency of the communities to return to a pH of 6.5 during daily dilution in the experiment. The eLV model is therefore a minimal modification of the gLV model that incorporates a single global environmental variable where each community is defined by both the species interaction matrix and the species-environment interactions.

Characterization of multistability and community type in the eLV model

To characterize the eLV model, we first partitioned the environmental variable *e* into three zones: acidic zone: e<-0.2; alkaline zone: e>0.2; neutral zone: $|e|\leq 0.2$, which is based on our simulation result. The environmental self-regulation factor δ is set to be 0.1. The environmental feedback on species growth g is sampled from uniform distribution [-1,1]. By increasing the environment modification strength $< |k| >$, we found that the bimodal distribution of single species e value emerged when $< |k| >$ is around $0.3 * \delta$ and the range of e value is around [-0.2, 0.2] (Figure S30). Therefore, we set -0.2 and 0.2 as separating points for the zones of environmental variable.

To further study the multistability in eLV model, we generated multiple time series from various initial conditions for randomly sampled communities and analyzed the differences in species abundances and environmental variables across all final stable states. To compare with the experiment, the species pool size in simulation is set to be 12. The environment feedback on species growth g_i is randomly sampled from uniform distribution [-1, 1], which simulate how strong the environment affects the species growth rate. The environmental modification by species k_i is randomly sampled from uniform distribution $[-\beta, \beta]$, where β can be varied to investigate the role of environmental modification strength, where $\beta = 2 < |k_i| >$. Similar with the gLV model, we varied species interaction strength $< \alpha_{ij} >$ and the environment modification strength $< |k_i| >$, across 11 values each. The interaction strength $< \alpha_{ij} >$ was sampled linearly in [0,1] (i.e., 0, 0.1, 0.2, ..., 1), while $< |k_i| >$ took logarithmically spaced values: 0, $0.1 * 2^{-6}, 0.1 * 2^{-5}, \dots, 0.1 * 2^{3}$. For each parameter set, we sampled 500 different communities and simulated their dynamics using the eLV model. The eLV model was solved using the fourth-order Runge-Kutta algorithm, simulating 1500 time units (step size = 0.1) to ensure the system reached a steady state. Similar with the gLV simulation, the community in eLV model is classified to be stable if the standard deviation of species abundance < 0.001 in the last 100 time units, and vice versa. Based on the environmental variable partition(acidic zone: e<-0.2; alkaline zone: e>0.2; neutral zone: $|e|\leq 0.2$), species abundance clustering analysis was used to identify compositional steady states within each zone, ultimately classifying the communities into four types: global stability (single zone, single steady state), functional bistability (two zones, single steady state each zone), compositional multistability (single zone, multiple steady states), hybrid multistability (multiple zones, multiple

steady states). Simulation results demonstrated that the eLV model could reproduce the four types observed in experiment. Our simulations revealed that functional bistability arises under strong environmental modification and intermediate species interaction strengths, compositional multistability occurs under weak environmental modification and strong species interaction, and hybrid multistability emerges under high species interaction combined with strong environmental modification (Figure S32).

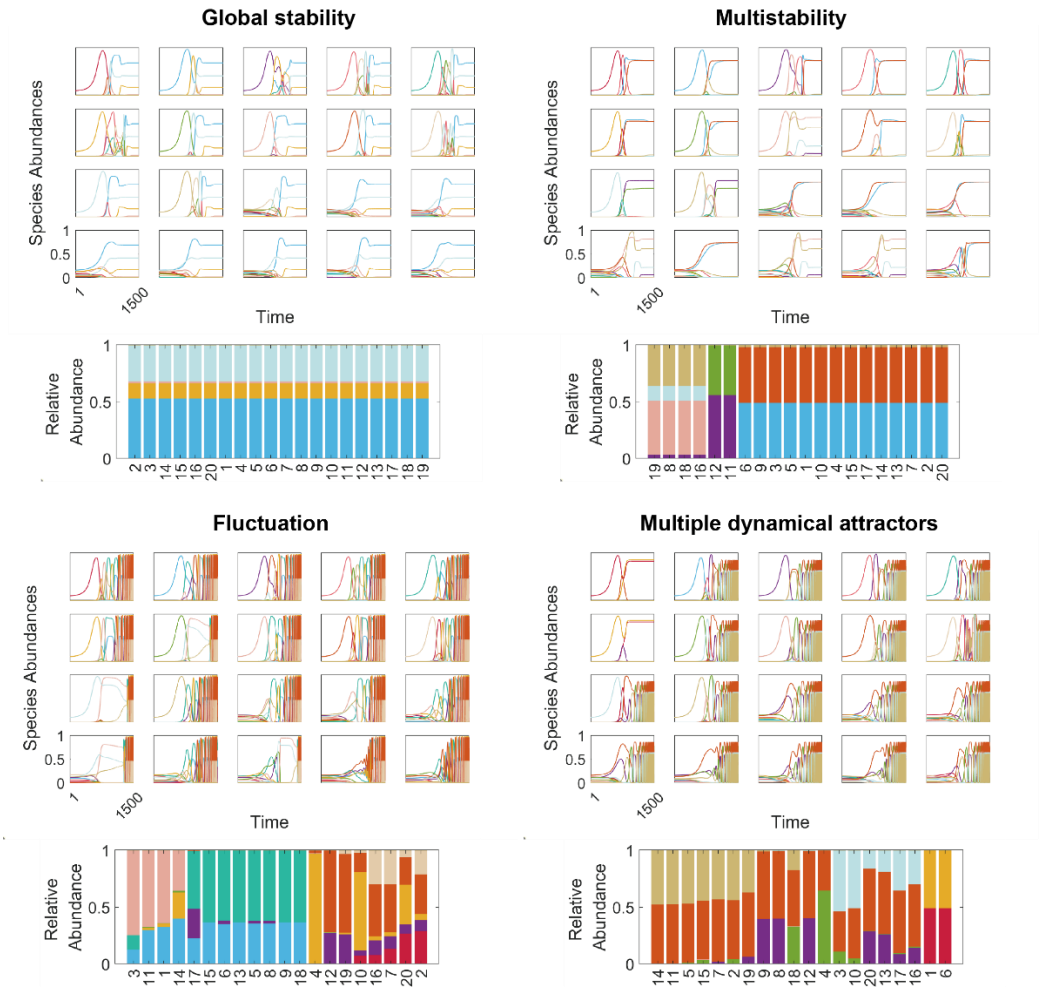

Figure S1. Global stability, multistability, fluctuation and multi-attractors in gLV communities. These four communities represent four types of outcomes: global stability, multistability, fluctuation and multiple dynamical attractors (fluctuation-stable). For each community, we plotted the abundances dynamics starting from 20 different initial species abundances, and clustered the final relative species abundances to compare different final dynamical states. In these figures, we tested 20 initial species abundances for each community which are all generated with species pool size 12 and mean interaction strength 1.

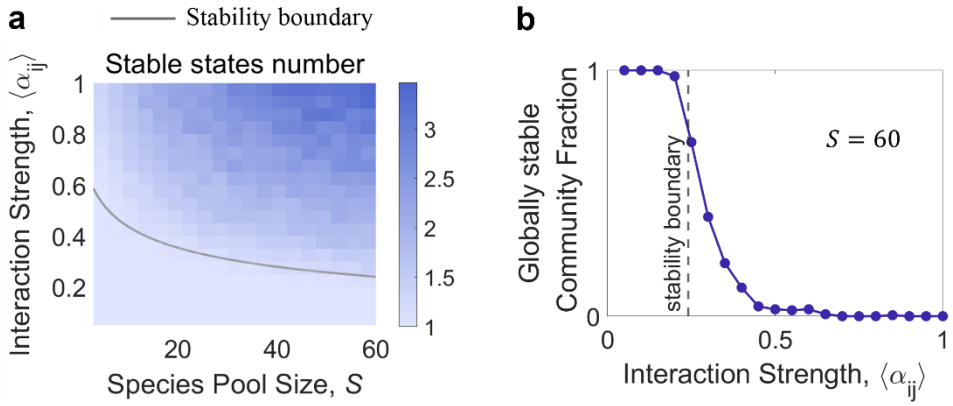

Figure S2. gLV prediction of the stability transition. (a)When the interaction strength and species pool size exceed a critical threshold, the system behavior undergoes a shift from global stability to the emergence of multiple stable states. The average states number can reach over three. (b) The communities with species pool size 60 exhibit a significant transition from global stability to multiple stable states. Compared to smaller species pool size (eg. *S*=12 in Fig. 1a and b), the interaction strength threshold for the transition ($< \alpha_{ij} > = 0.24$) is smaller and the transition is sharper.

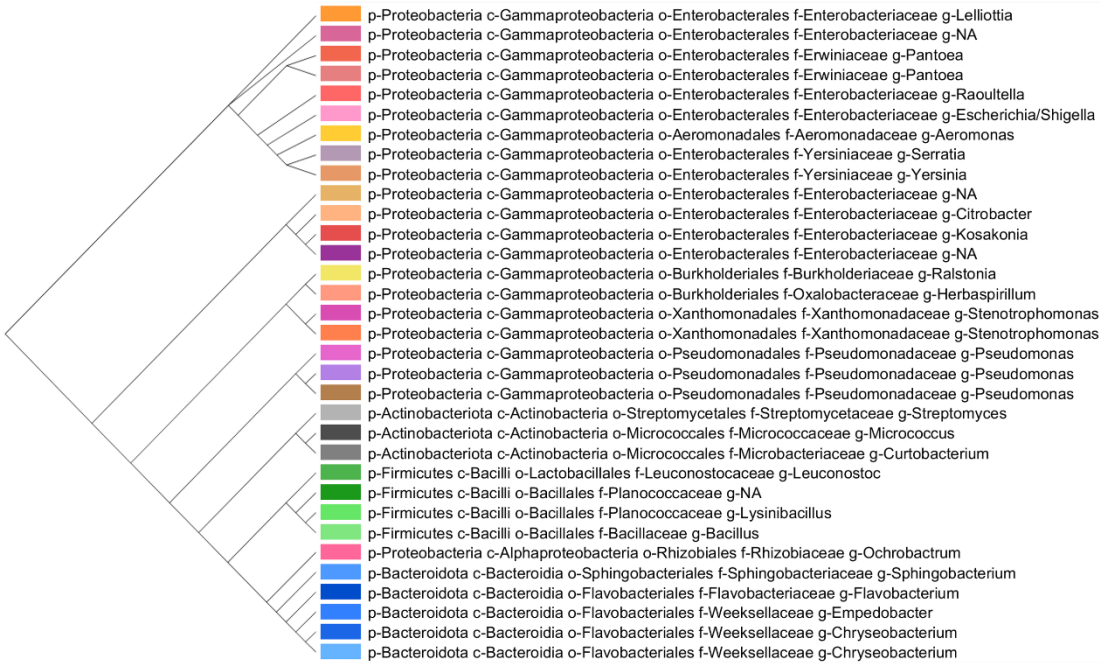

Figure S3. The phylogenetic tree and taxonomy identity of 33 distinct species. The identities have been inferred from the ASV of 16S rRNA sequencing samples taken from monocultures, which allow the classification of the 54 isolates (33 distinct species) down to the genus level. Colors are consistent with those in the main text and other supplementary figures. The phylogenetic tree analysis was performed using MAFFT for sequence alignment, IQ-TREE for maximum-likelihood tree construction, and iTOL for visualization. It shows relative phylogenetic distance between the 33 distinct species. The library spans 4 different phylums, 12 different orders and 18 different families. Colors are assigned by phylum: Bacteroidota in blue, Firmicutes in green, Actinobacteriota in grey, and Proteobacteria in a range of warm tones (red, orange, brown, pink).

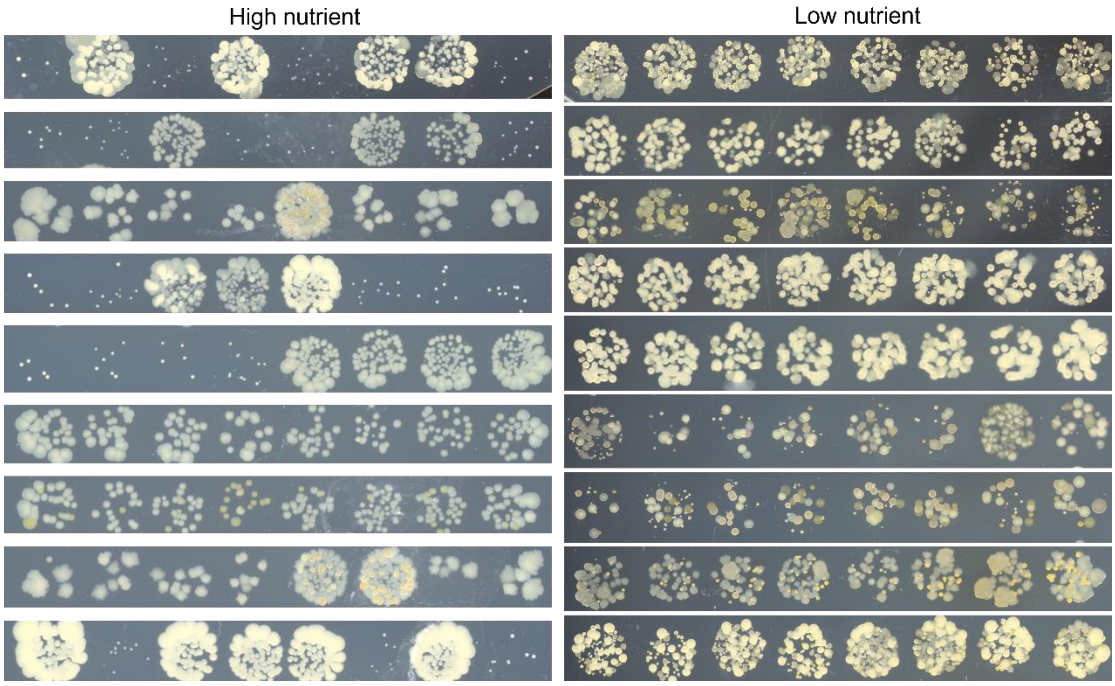

Figure S4. The colony morphology of eight replicates in each of the nine communities in both low and high nutrient conditions. Each row shows the plating result of eight replicates of a single community in either high or low nutrient conditions. The selected communities display obvious multistability, with further species abundances information inferred by sequencing result shown in Figure S6-S7. Here, each colony shows the species composition of 1μL diluted (10^5 ×) community on the last day.

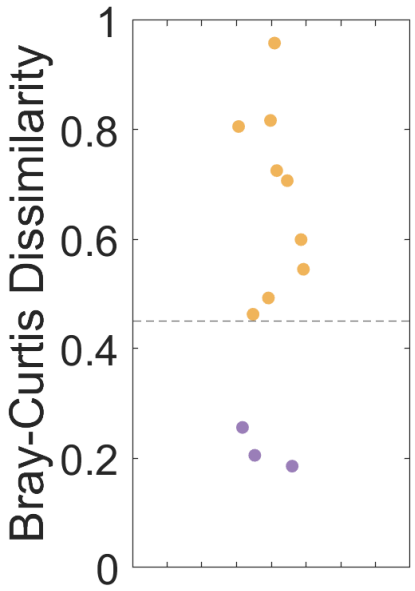

Figure S5. Bray-Curtis dissimilarity of time series during last 3 days from 12 stable or fluctuating communities. We chose 12 communities with same species pool but starting from different initial abundances, where three communities are stable and nine are fluctuating (Figure 2). We calculated the maximum Bray-Curtis dissimilarity between species abundances of day5, day6, and day7, which shows clear distinction between stable and fluctuating communities. Based on this metric, we set the multistable threshold to be 0.45 to distinguish whether the final states of a single community shows global stability or multistability.

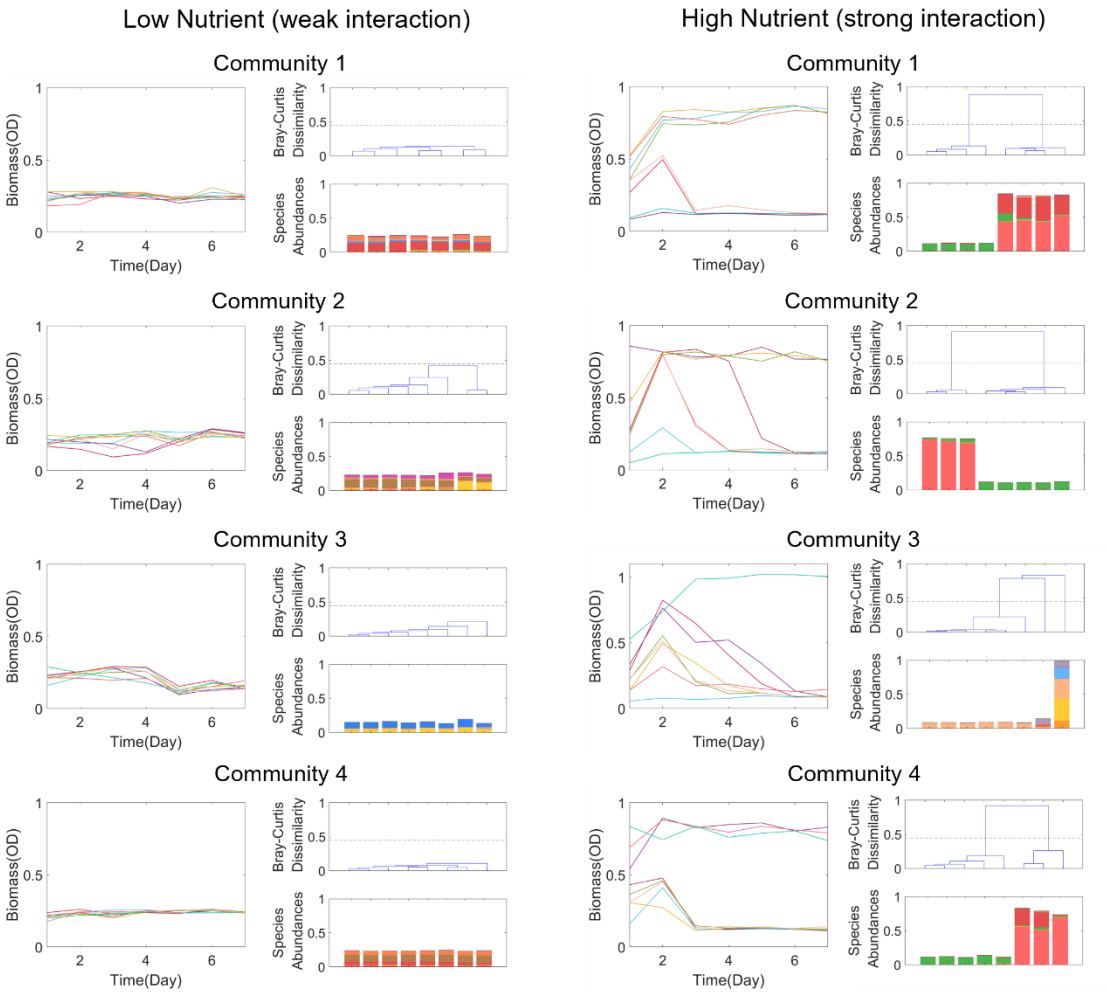

Figure S6. The transition from global stability to multistability in the nine experimental communities (S = 24). Four communities with species pool size 24 are shown here. Each row represents one community with same species pool, cultured in both low and high nutrient communities. As the biomass (OD) time series show, all communities have reached stable states on day 7. The species abundances are calculated based on the community total biomass and 16S sequencing result, where different colors represent different species (Figure S3). Based on Bray-Curtis dissimilarity between each pair of replicates, we performed hierarchical clustering to calculate the states number (cutoff threshold is 0.45, consistent with main text). All four communities in low-nutrient (weak interaction) conditions reached a single stable state regardless of their initial species abundances, whereas in high-nutrient conditions all the four communities exhibited multiple stable states on the final day.

$S = 12$

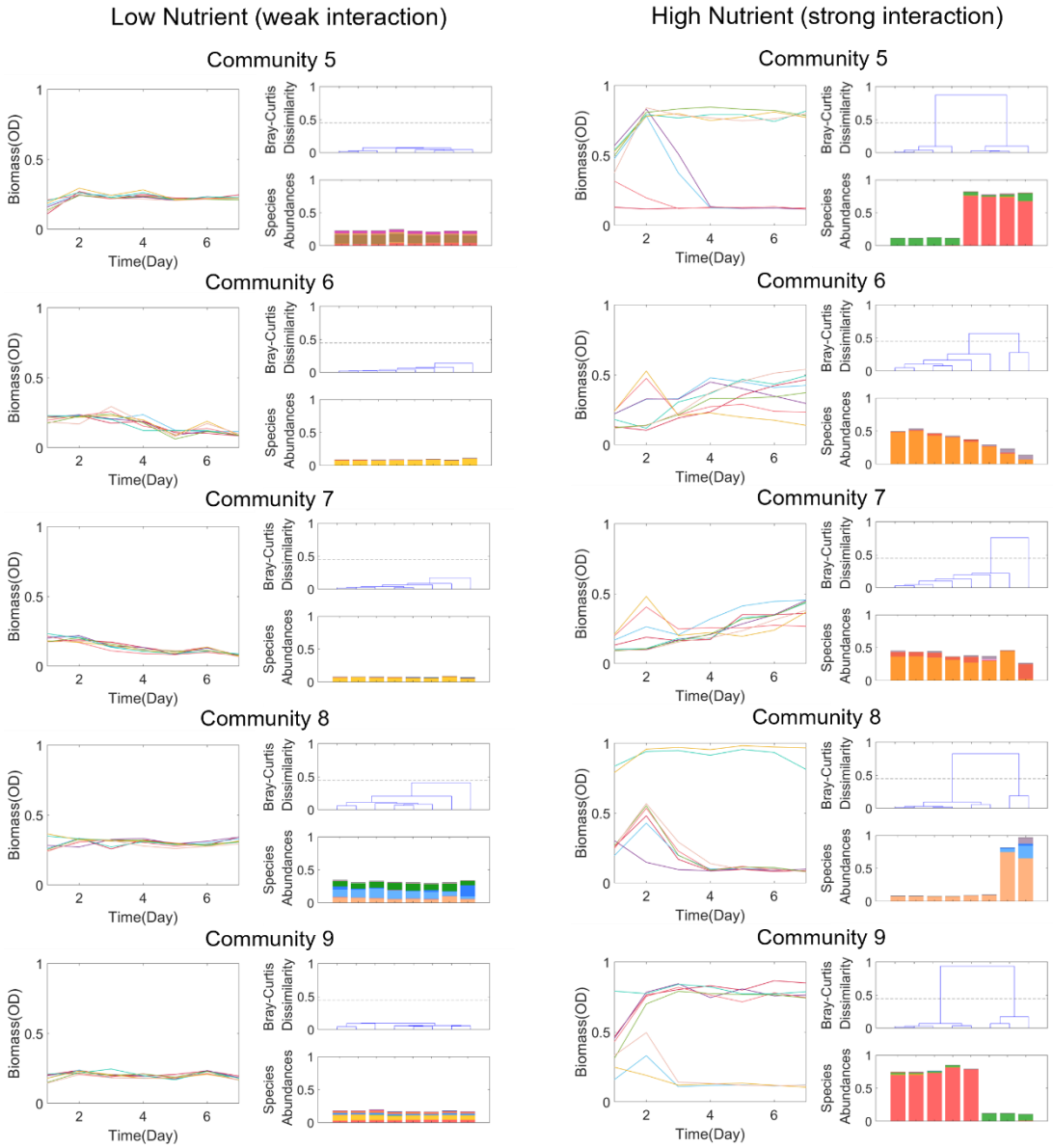

Figure S7. The transition from global stability to multistability in the nine experimental communities (*S* = 12). Five communities with species pool size 12 are shown here. Each row represents one community with same species pool, cultured in both low and high nutrient communities. As the biomass (OD) time series show, all communities have reached stable states on day 7. The species abundances are calculated based on the community total biomass and 16S sequencing result, where different colors represent different species (Figure S3). Based on Bray-Curtis dissimilarity between each pair of replicates, we performed hierarchical clustering to calculated the states number (cutoff threshold is 0.45, consistent with main text). All five communities in low-nutrient (weak interaction) conditions reached a single stable state regardless of their initial species abundances, whereas in high-nutrient conditions all the five communities exhibited multiple stable states on the final day.

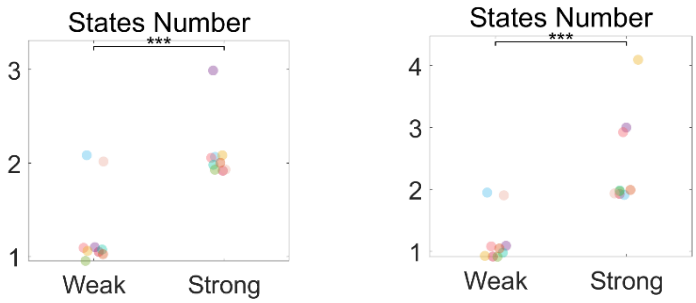

Figure S8. States number of the nine communities under different threshold. The states number is calculated based on the hierarchical clustering in species absolute abundances (normalized by biomass (OD)). In the main text, the cutoff threshold in the hierarchical clustering for different stable states is 0.45. If we lower the threshold to 0.3(left panel), two communities in low nutrient condition start to exhibit bi-stability, but the difference between weak and strong interaction remain significant. If we further lower the threshold to 0.25(right panel), communities in high nutrient conditions start to exhibit more stable states.

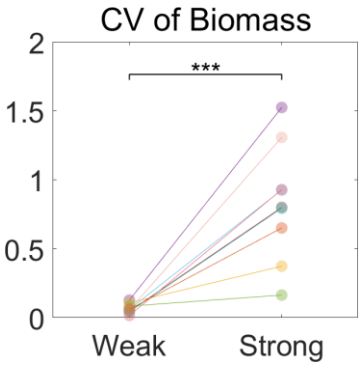

Figure S9. The variation in total biomass increased in the high-nutrient condition. The coefficient of variation (CV) of community biomass was calculated as the ratio of the standard deviation (σ) to the mean (μ) across all eight replicates with different initial species abundances. This metric quantifies the relative variability in biomass measurements, enabling comparison across samples with differing total biomass. The result shows that the CV in total biomass increased substantially across all nine communities as species interaction strength increases.

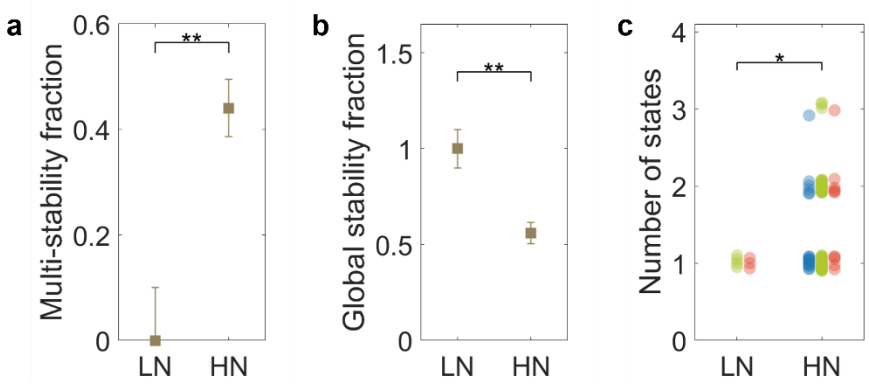

Figure S10. Comparison of all communities in low and high nutrient. Apart from the nine communities tested in both low and high nutrient conditions, we also have another 70 communities cultured in high nutrient conditions with sequencing results. Using the clustering methods and threshold in main text, we compared the 9 communities in low nutrient(LN) conditions and 79 communities in high nutrient(HN) conditions. (a, b) We found that 0±10% communities in low nutrient (weak interaction) exhibit multistability, while 44.0±5.4% communities in high nutrient (strong interaction) exhibit multistability ($p = 0.0099$). (c) The states number in high nutrient ranges from one to three, which is a significant increase from only one state in weak species interaction ($p = 0.0165$).

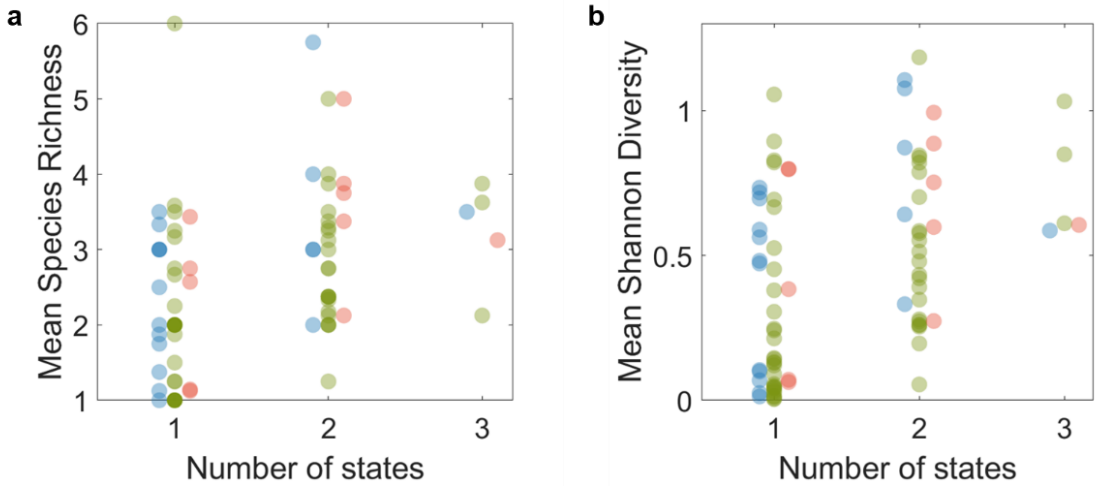

Figure S11. Positive correlation between the number of states and species richness. (a) The number of states is positively correlated with mean species richness under high nutrient (strong interaction) condition (corrcoef = 0.4217, p = 6.4762e-05). Here, the species richness is calculated by surviving species number (the number of species whose relative abundance is above survival threshold 0.01). The mean species richness for a community is the average species richness over all replicates for a single community. (b) We also calculated the Shannon diversity of species abundances, and the positive correlation is robust. The number of states is positively correlated with mean Shannon Diversity under high nutrient (strong interaction) condition (corrcoef = 0.4328, p = 3.9331e-05).

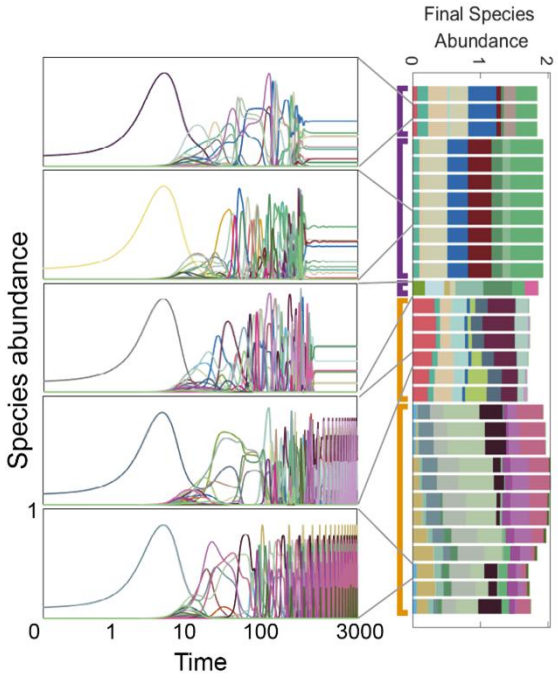

Figure S12. Multiple dynamical attractors with large species pool size predicted by the gLV model. When the species pool size is large, complex dynamical behaviors can be observed. For instance, in a gLV model with species pool size $S = 60$ and interaction strength $\alpha_{ij} = 0.8$, simulations were conducted with 30 different initial species abundances. By calculating the average species abundances over the last period of time series (1400–1500 time units), the mean final species abundances were obtained, as shown in the right panel histogram. Based on these results, the community attractors can be classified into three stable states and two fluctuating attractors. Since averaging reduces the large fluctuations caused by the temporal variations of the fluctuating attractors, the differences in species composition and abundances between the two types of fluctuating attractors become more obvious.

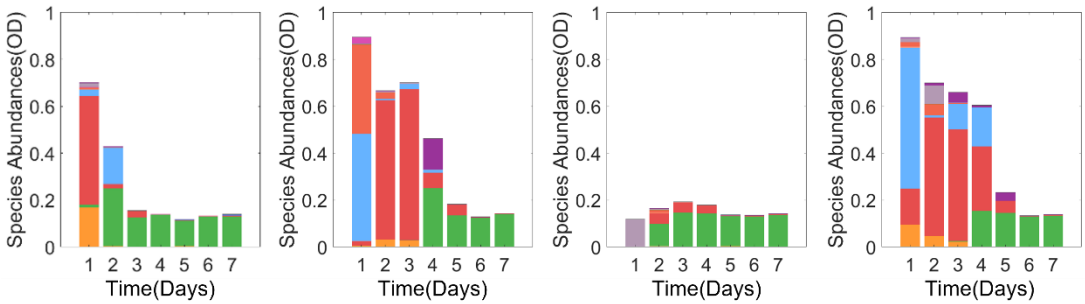

Figure S13. Experimental communities showing time series of stable states. This figure shows an example community exhibiting global stability. Four time series show the assembly dynamics of the same community from four different initial species abundances. In this community, many different initial abundances all converge to same biomass, species composition and abundance on the final day, showing global stability.

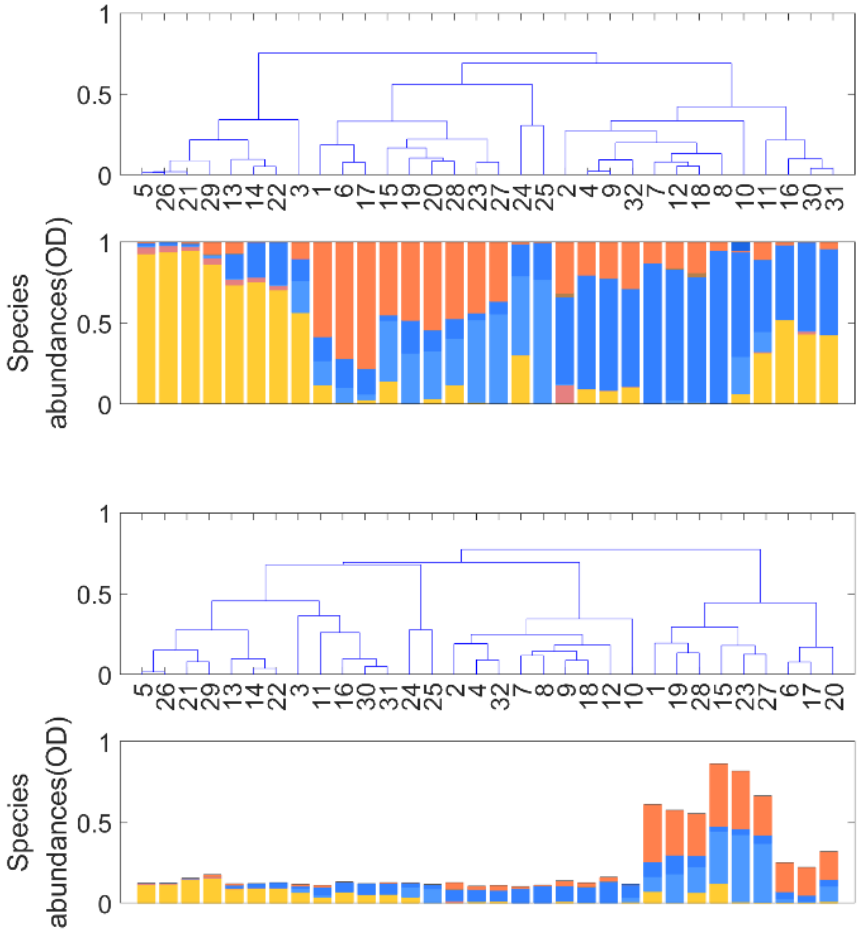

Figure S14. The final species abundances (day 7) of single community with multiple attractors. Community IV can either converge to multiple different stable states or fluctuate depending on initial species abundances (Figure 2a). Here we show the final day species abundances for all the 32 replicates in community IV that we tested in our experiments. The clustering clearly shows that there are at least four different clusters of attractors, among which some are stable, some are fluctuating (Figure 2a).

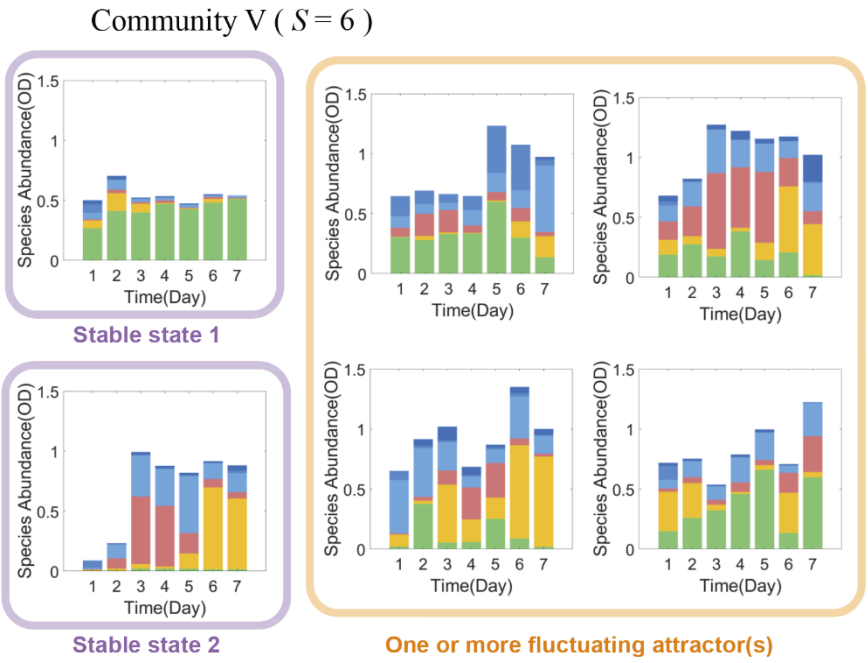

Figure S15. Other example experimental communities for multiple attractors. Community V with species pool size 6 is another experimental community showing multiple dynamical attractors. This community can either converge to stable states or fluctuate depending on initial species abundances. Among the six initial species abundances we tested in our experiment, two converge to stable states and four initial species abundances lead to fluctuating dynamics.

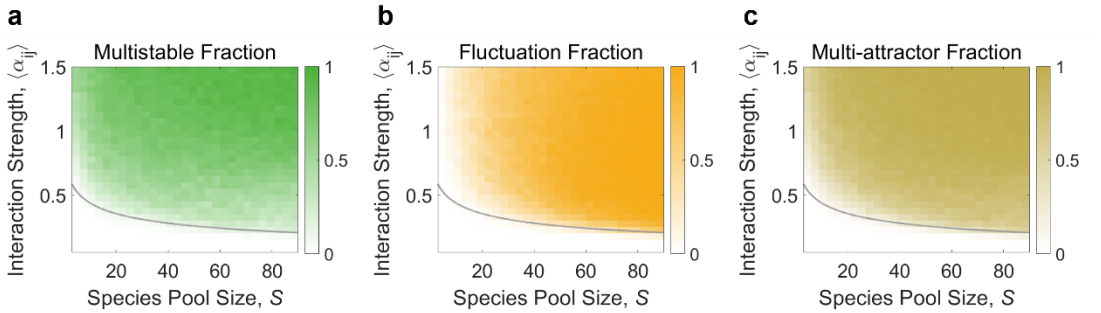

Figure S16. Phase diagrams for the communities in gLV model. (a) In our simulations, multi-stable communities refer to the communities with multiple stable states, regardless of whether it could fluctuate under some initial species abundances. Communities with multiple stable states increases as either species pool size or interaction strength increases. (b) Fluctuation communities refer to the communities that could go to fluctuation under certain initial species abundances. Communities with fluctuating attractors increases as either species pool size or interaction strength increases. (c) Multi-attractor communities refer to the communities with multiple dynamical attractors, such as multiple stable states or having both stable and fluctuating states.

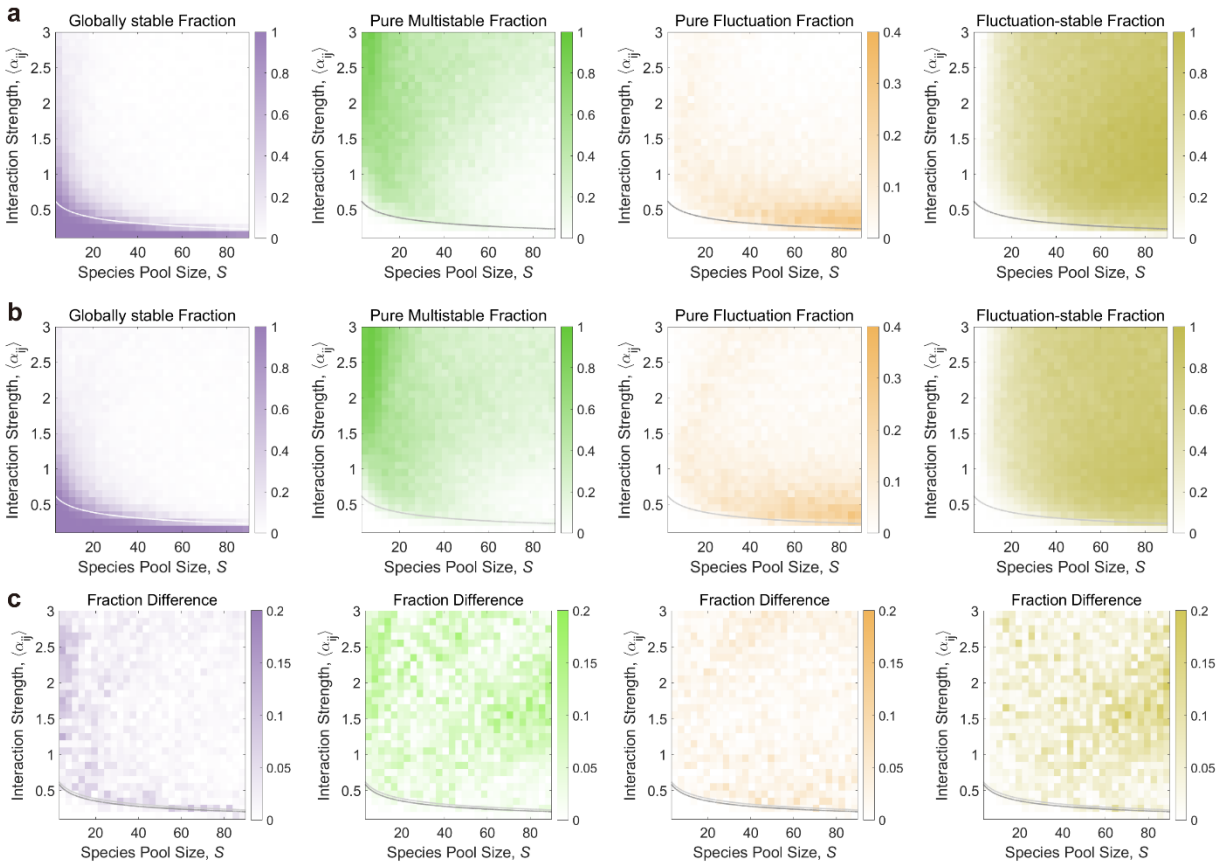

Figure S17. Comparison between phase diagrams of gLV communities with different α_{ij} distributions. (a) The phase diagrams for gLV model, with alpha_ij randomly sampled from uniform distribution. (b) The phase diagrams with alpha_ij randomly sampled from Gaussian distribution ($std(\alpha_{ij}) = \langle \alpha_{ij} \rangle / \sqrt{3}$). (c) The difference between the fractions of two distributions, indicating that the results are similar across different distributions.

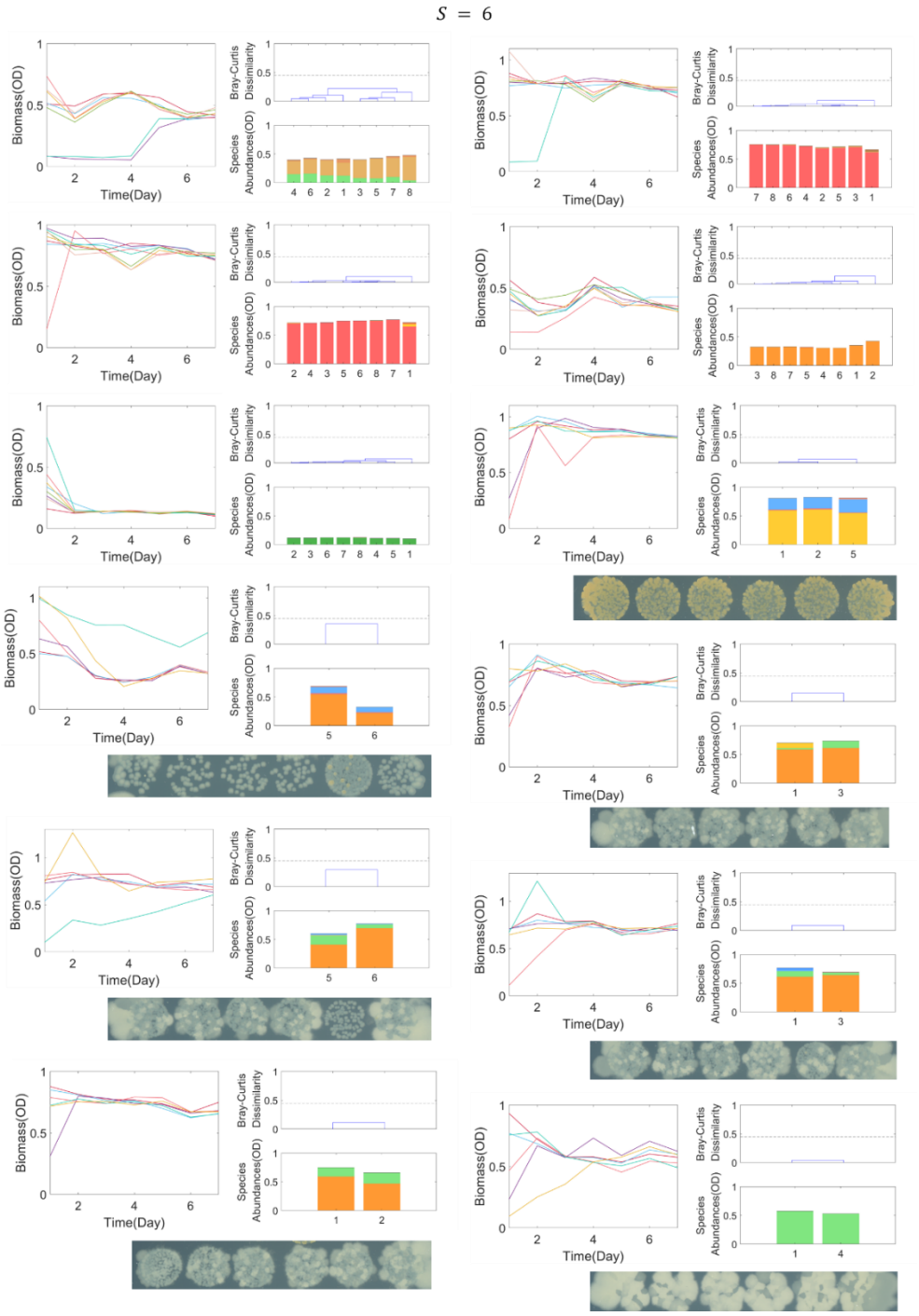

Figure S18. Biomass time series and final species abundances of global-stable communities ($S = 6$). All global-stable communities with species pool size 6, dilution factor 10^3 are shown here (12 communities). As the biomass (OD) time series show, all communities have reached stable states on day 7. The species abundances are calculated based on the community total biomass and 16S sequencing result, where different colors represent different species (Figure S3). Based on Bray-Curtis dissimilarity between each pair of replicates, we performed hierarchical clustering to calculate the states number (cutoff threshold is 0.45, consistent with main text). Each community shown here has a single stable state. Some communities had sequencing data for only two or three replicates, but we classified them as globally stable by incorporating both plating and sequencing results.

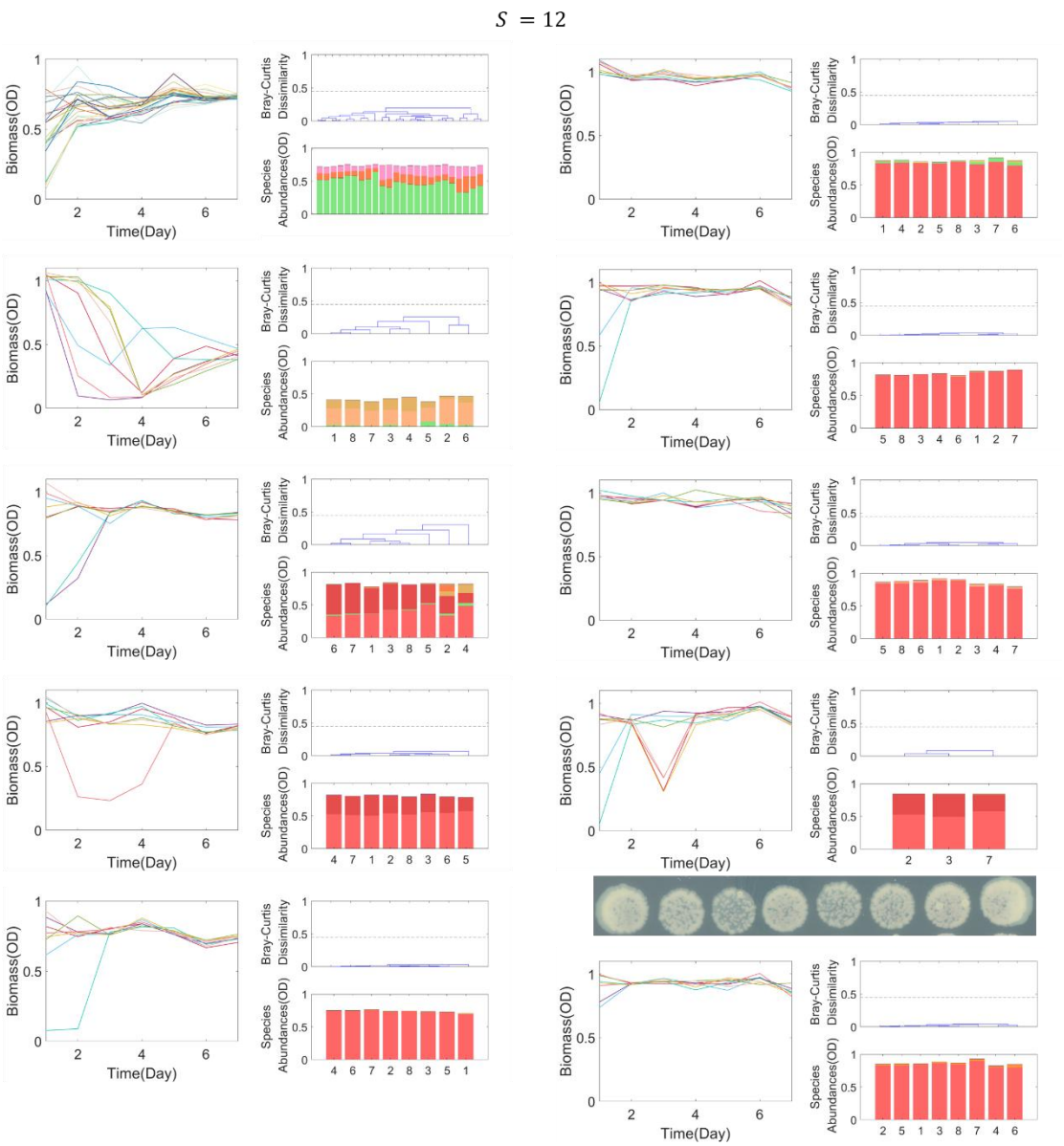

Figure S19. Biomass time series and final species abundances of globally stable communities ($S = 12$). Ten global-stable communities with species pool size 12, dilution factor 10^3 are shown here (out of 17 communities). As the biomass (OD) time series show, all communities have reached stable states on day 7. The species abundances are calculated based on the community total biomass and 16S sequencing result, where different colors represent different species (Figure S3). Based on Bray-Curtis dissimilarity between each pair of replicates, we performed hierarchical clustering to calculate the states number (cutoff threshold is 0.45, consistent with main text). Each community shown here has a single stable state. Some communities had sequencing data for only two or three replicates, but we classified them as globally stable by incorporating both plating and sequencing results.

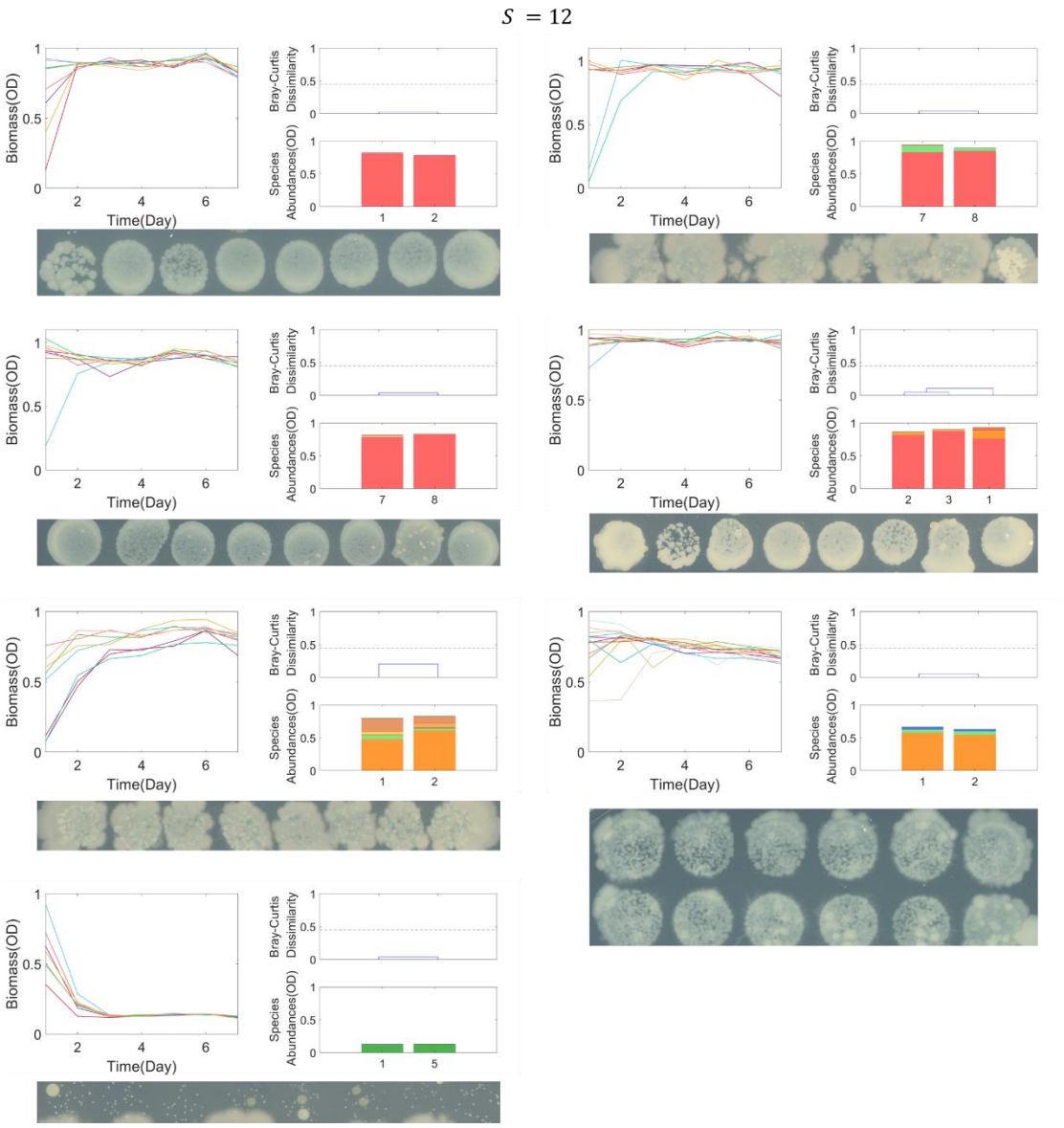

Figure S20. Biomass time series and final species abundances of globally stable communities ($S = 12$). Seven global-stable communities with species pool size 12, dilution factor 10^3 are shown here (out of 17 communities). As the biomass (OD) time series show, all communities have reached stable states on day 7. The species abundances are calculated based on the community total biomass and 16S sequencing result, where different colors represent different species (Figure S3). Based on Bray-Curtis dissimilarity between each pair of replicates, we performed hierarchical clustering to calculate the states number (cutoff threshold is 0.45, consistent with main text). Each community shown here has a single stable state. Some communities had sequencing data for only two or three replicates, but we classified them as globally stable by incorporating both plating and sequencing results.

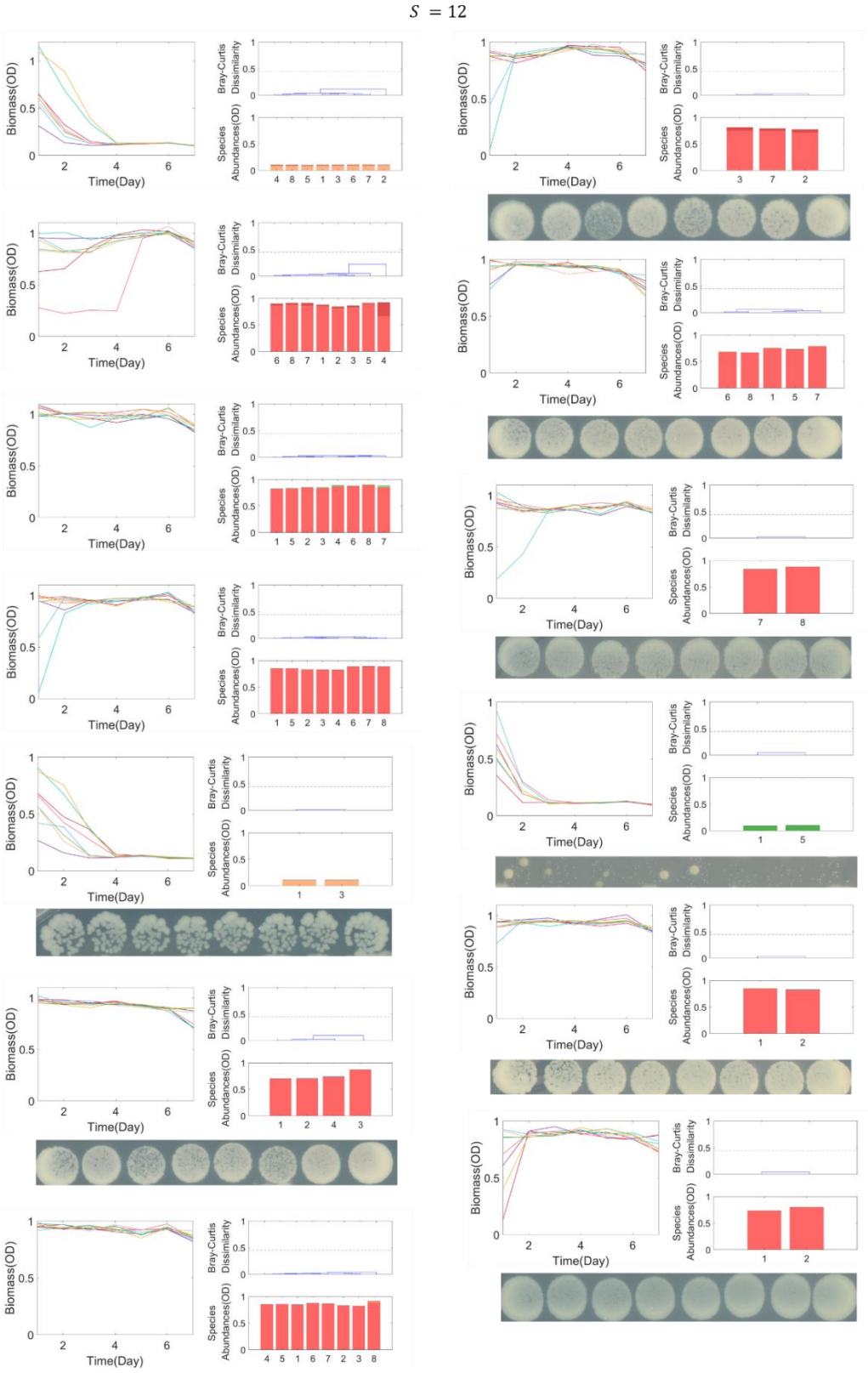

Figure S21. Biomass time series and final species abundances of globally stable communities ($S = 12, Dilution = 10^5$). All global-stable communities with species pool size 12, dilution factor 10^5 are shown here (13 communities). As the biomass (OD) time series show, all communities have reached stable states on day 7. The species abundances are calculated based on the community total biomass and 16S sequencing result, where different colors represent different species (Figure

S3). Based on Bray-Curtis dissimilarity between each pair of replicates, we performed hierarchical clustering to calculate the states number (cutoff threshold is 0.45, consistent with main text). Each community shown here has a single stable state. Some communities had sequencing data for only two or three replicates, but we classified them as globally stable by incorporating both plating and sequencing results.

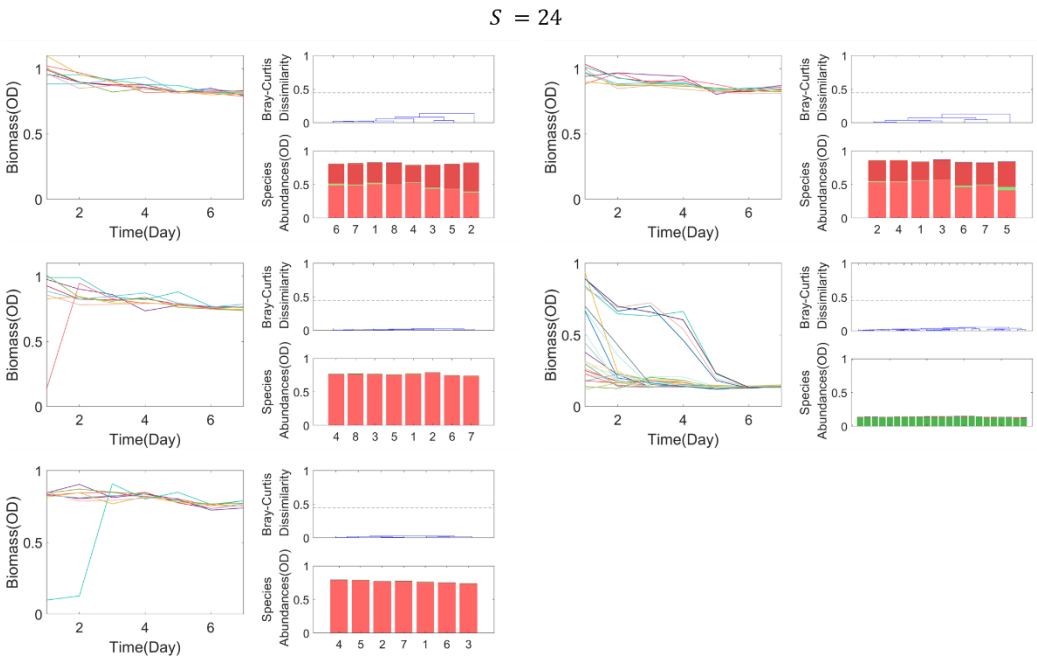

Figure S22. Biomass time series and final species abundances of globally stable communities ($S = 24, Dilution = 10^3$). All global-stable communities with species pool size 24, dilution factor 10^3 are shown here (5 communities). As the biomass (OD) time series show, all communities have reached stable states on day 7. The species abundances are calculated based on the community total biomass and 16S sequencing result, where different colors represent different species (Figure S3). Based on Bray-Curtis dissimilarity between each pair of replicates, we performed hierarchical clustering to calculated the states number (cutoff threshold is 0.45, consistent with main text). Each community shown here has a single stable state.

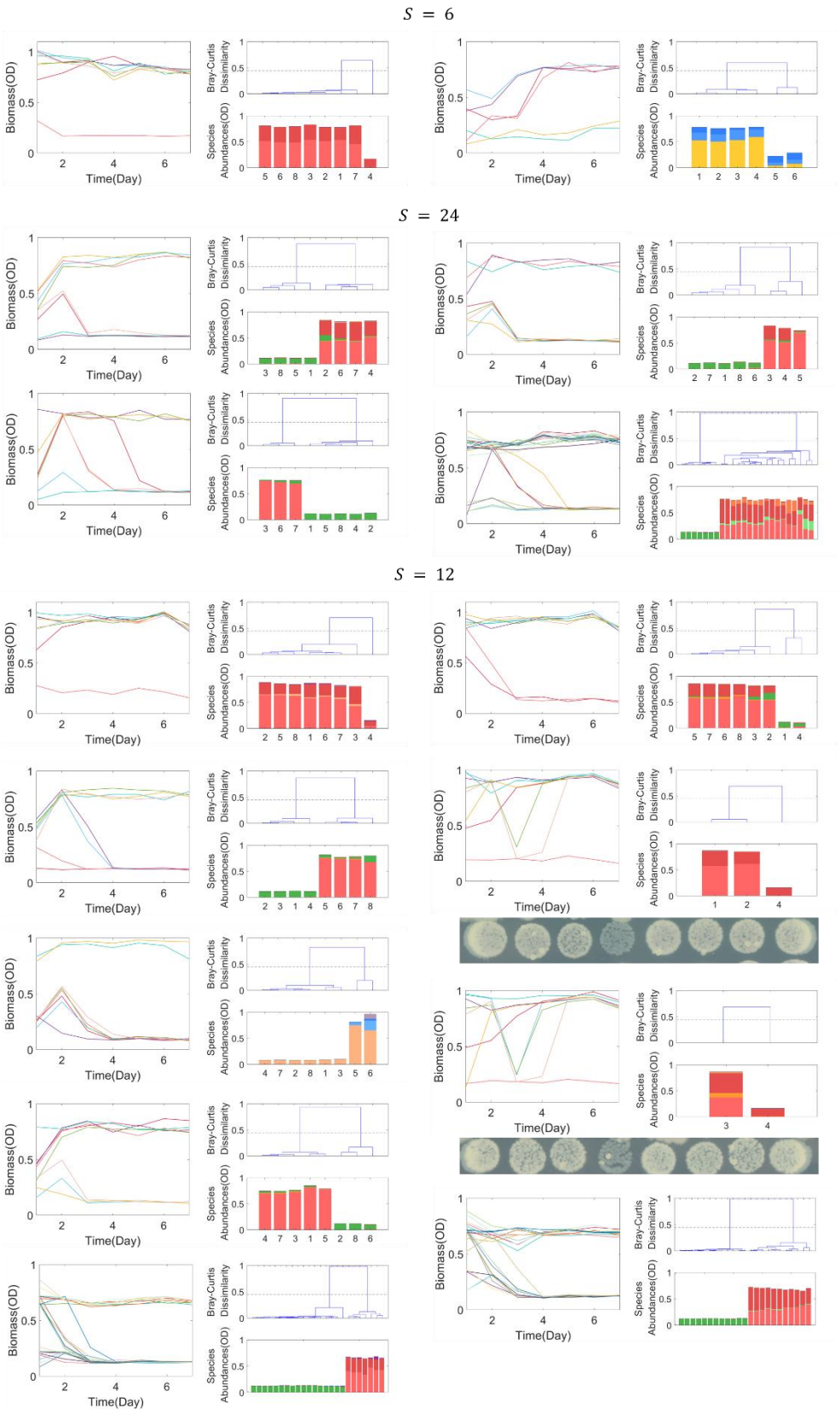

Figure S23. Biomass time series and final species abundances of functional bistable communities ($Dilution = 10^3$). All functional bistable communities with dilution factor 10^3 are shown here (13 communities). As the biomass (OD) time series show, all communities have reached stable states on day 7. The species abundances are calculated based on the community total biomass

and 16S sequencing result, where different colors represent different species (Figure S3). Based on Bray-Curtis dissimilarity between each pair of replicates, we performed hierarchical clustering to calculated the states number (cutoff threshold is 0.45, consistent with main text). Each community shown here has two distinct stable states. Some communities had sequencing data for only two or three replicates, but we classified them as functional bistable by incorporating both plating and sequencing results.

$S = 12$

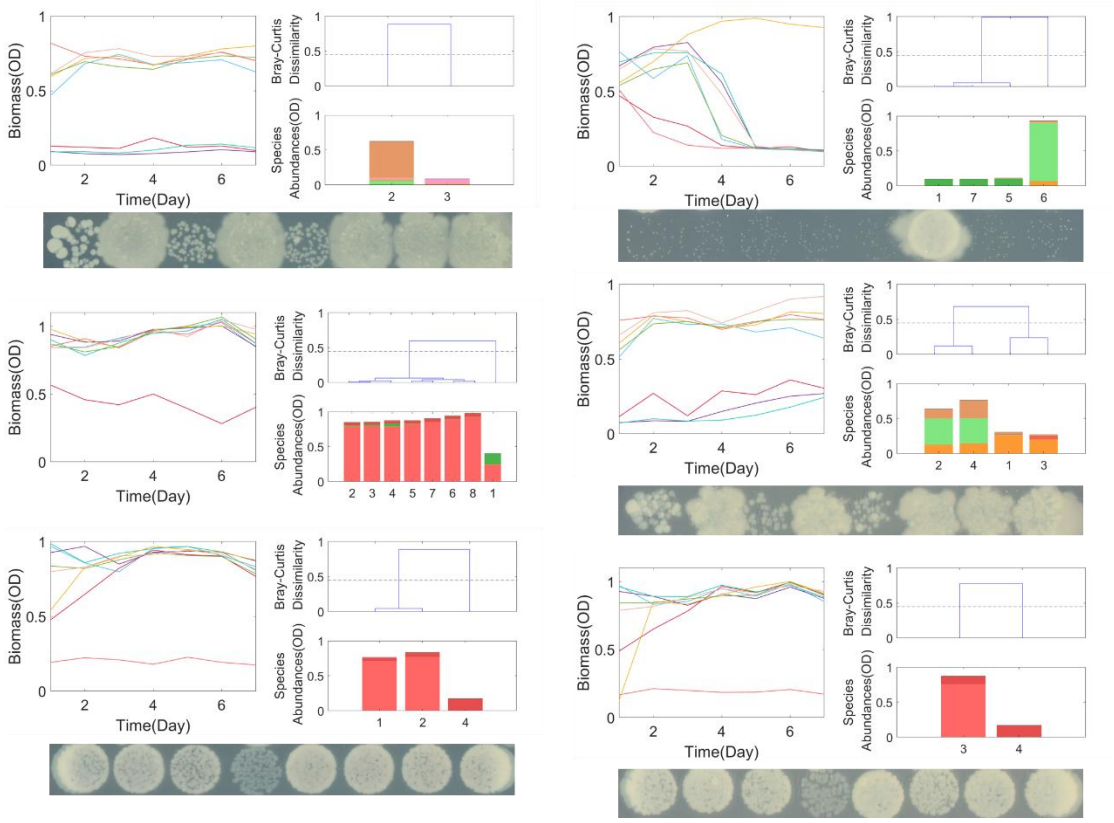

Figure S24 Biomass time series and final species abundances of functional bistable communities ($Dilution = 10^5$). All functional bistable communities with dilution factor 10^5 are shown here (6 communities). As the biomass (OD) time series show, all communities have reached stable states on day 7. The species abundances are calculated based on the community total biomass and 16S sequencing result, where different colors represent different species (Figure S3). Based on Bray-Curtis dissimilarity between each pair of replicates, we performed hierarchical clustering to calculated the states number (cutoff threshold is 0.45, consistent with main text). Each community shown here has two distinct stable states. Some communities had sequencing data for only two to four replicates, but we classified them as functional bistable by incorporating both plating and sequencing results.

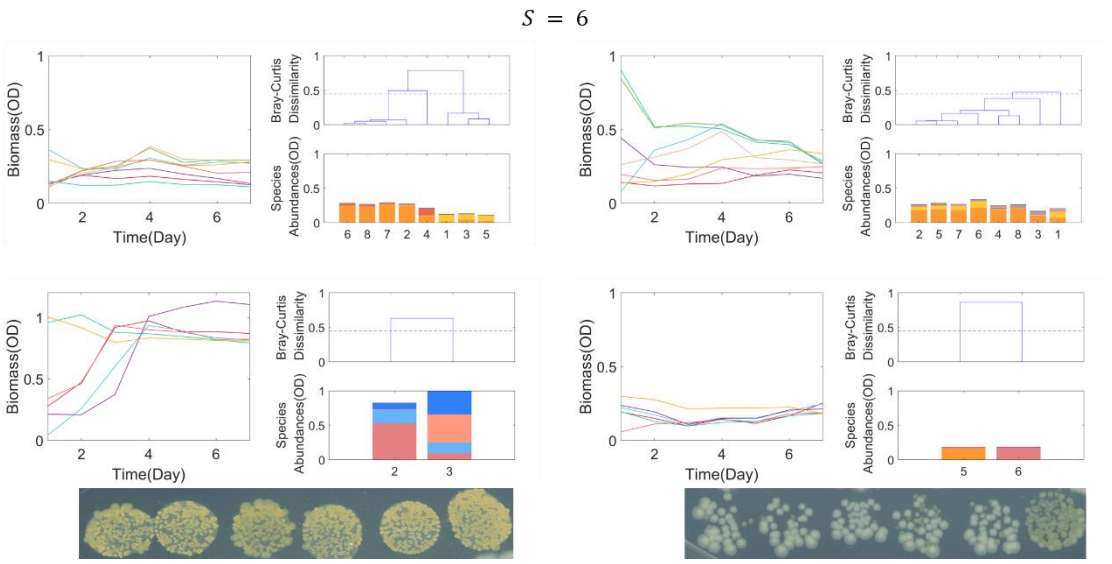

Figure S25. Biomass time series and final species abundances of compositional multistable communities ($S = 6$). All compositional multistable communities with species pool size 6, dilution factor 10^5 are shown here (4 communities). As the biomass (OD) time series show, all communities have reached stable states on day 7. The species abundances are calculated based on the community total biomass and 16S sequencing result, where different colors represent different species (Figure S3). Based on Bray-Curtis dissimilarity between each pair of replicates, we performed hierarchical clustering to calculated the states number (cutoff threshold is 0.45, consistent with main text). Each community shown here has two to three distinct stable states. Some communities had sequencing data for only two to four replicates, but we classified them as compositional multistable by incorporating both plating and sequencing results.

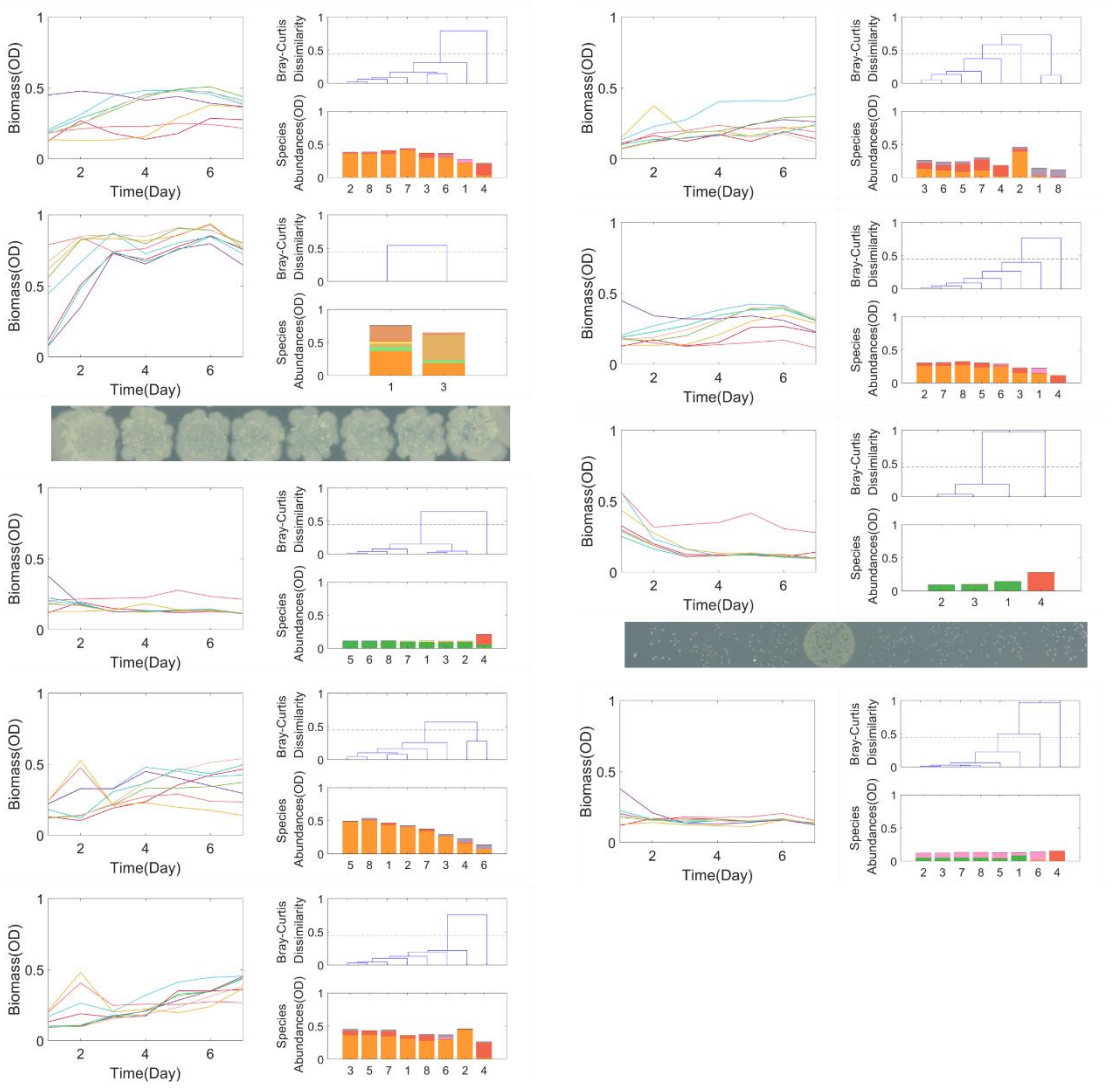

Figure S26. Biomass time series and final species abundances of compositional multistable communities ($S = 12$). All compositional multistable communities with species pool size 12 are shown here (9 communities). The first column shows five communities with dilution factor 10^3, and the second column shows four communities with dilution factor 10^5. As the biomass (OD) time series show, all communities have reached stable states on day 7. The species abundances are calculated based on the community total biomass and 16S sequencing result, where different colors represent different species (Figure S3). Based on Bray-Curtis dissimilarity between each pair of replicates, we performed hierarchical clustering to calculated the states number (cutoff threshold is 0.45, consistent with main text). Each community shown here has two to three distinct stable states. Some communities had sequencing data for only two to four replicates, but we classified them as compositional multistable by incorporating both plating and sequencing results.

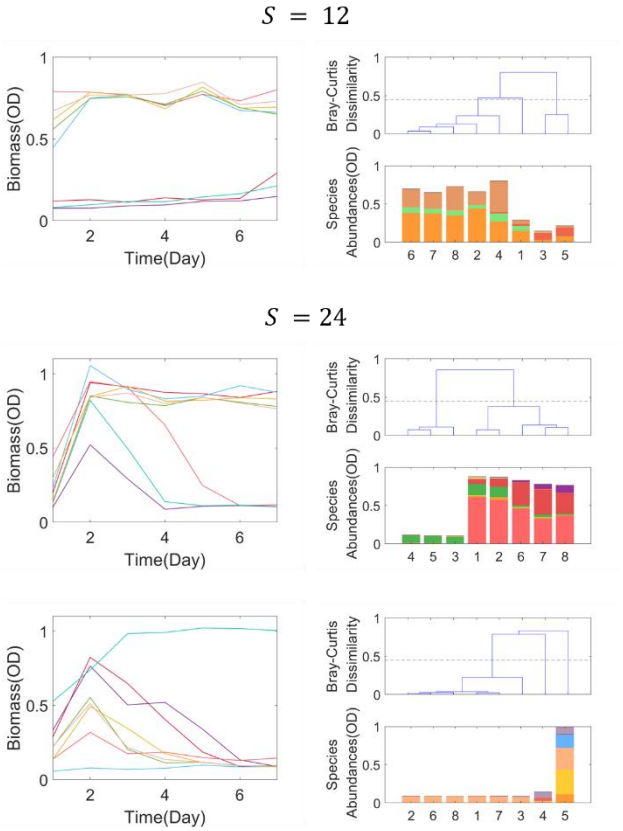

Figure S27. Biomass time series and final species abundances of hybrid multistable communities. All hybrid multistable communities are shown here (3 communities). As the biomass (OD) time series show, all communities have reached stable states on day 7. The species abundances are calculated based on the community total biomass and 16S sequencing result, where different colors represent different species (Figure S3). Based on Bray-Curtis dissimilarity between each pair of replicates, we performed hierarchical clustering to calculated the states number (cutoff threshold is 0.45, consistent with main text). The first community ($S = 12, D = 10^5$) is classified as hybrid multistability using the quantification for the maximum difference between biomass and species abundances shown in main text (Figure 4g). Based on the hierarchical clustering, the eight stable replicates are classified as 3 different states. The second community ($S = 24, D = 10^5$) is a community in between functional bistability and hybrid multistability. In our quantification for the maximum difference between biomass and species abundances, it is classified as hybrid multistability but on the boundary. Using the states number threshold in the main text, this community has only two states, but if the states number threshold is lowered to 0.4, it can be identified as 3 states. Therefore, together with the recurrence of each state in this community, we classified this community as hybrid multistability. The third community ($S = 24, D = 10^3$) is the example community in the main text (Figure 4f), showing obvious three different states with hybrid multistability, supported by both states clustering and dissimilarity quantification.

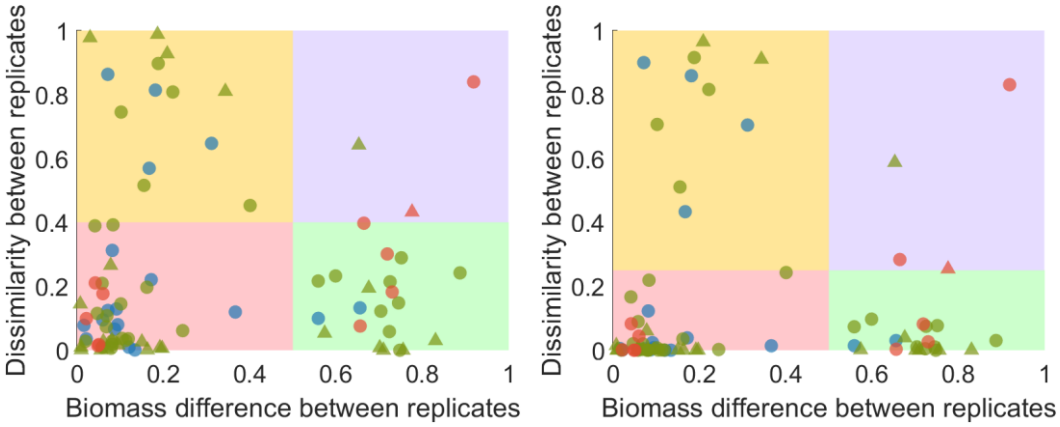

Figure S28. Several quantitative classifications of community types. (a)We tested Bray-Curtis dissimilarity of species relative abundances (threshold 0.4) to classify the experimental communities, the classification of communities (except for few communities near the boundary) remains robust. (b) We also tested other normalized dissimilarity metrics, such as correlation distance of absolute species abundances, with threshold 0.25, the classification remains largely similar.

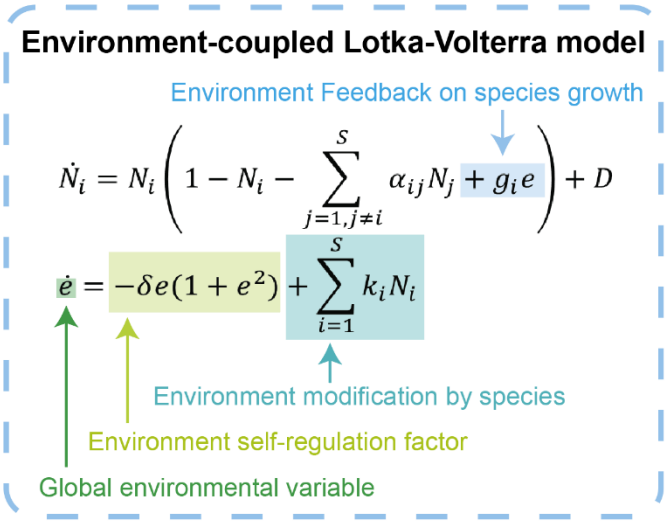

Figure S29. The environment-coupled Lotka-Volterra(eLV) model. We developed the environment-coupled Lotka-Volterra (eLV) model, which extends the generalized Lotka-Volterra (gLV) model by incorporating a global environmental variable e and its associated dynamical equation. The environmental variable, which represents shared environmental factors such as pH, is influenced by species in the community and, in turn, modifies species growth rates. Additionally, the global environmental variable has self-regulation, where the linear term leads to relaxation to an equilibrium at rate δ and the cubic restoring term sets a scale for typical variation.

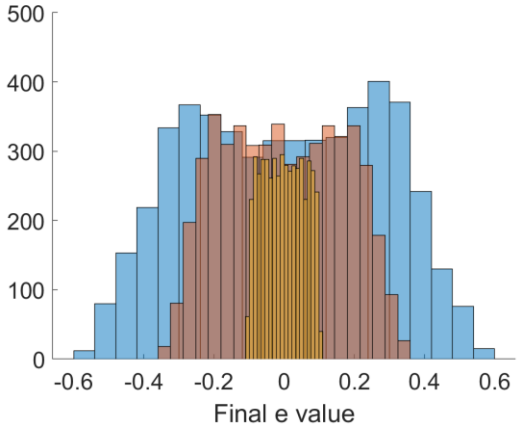

Figure S30. The bimodal distribution of environmental variable and the zone partition in the eLV model. When $< |k| > = 0.1 * \delta$, the environmental variable (e value) exhibits no obvious bimodal distribution as the environmental variable is weakly affected by the species (orange). When $< |k| > = 0.5 * \delta$, the e value shows significant bimodal distribution as it is strongly modified by the species(blue). By increasing the environment modification strength $< |k| >$ from $0.1* \delta$ to $0.5* \delta$, we found that the bimodal distribution of environmental variable (e value) emerged when $< |k| >$ is around 0.3 (red) and the range of e value is around [-0.2, 0.2]. Here, $\delta = 0.1$. Based on this, we partitioned the e value into three zones: acidic (e value<-0.2), neutral (-0.2<e value<0.2), alkaline (e value>0.2).

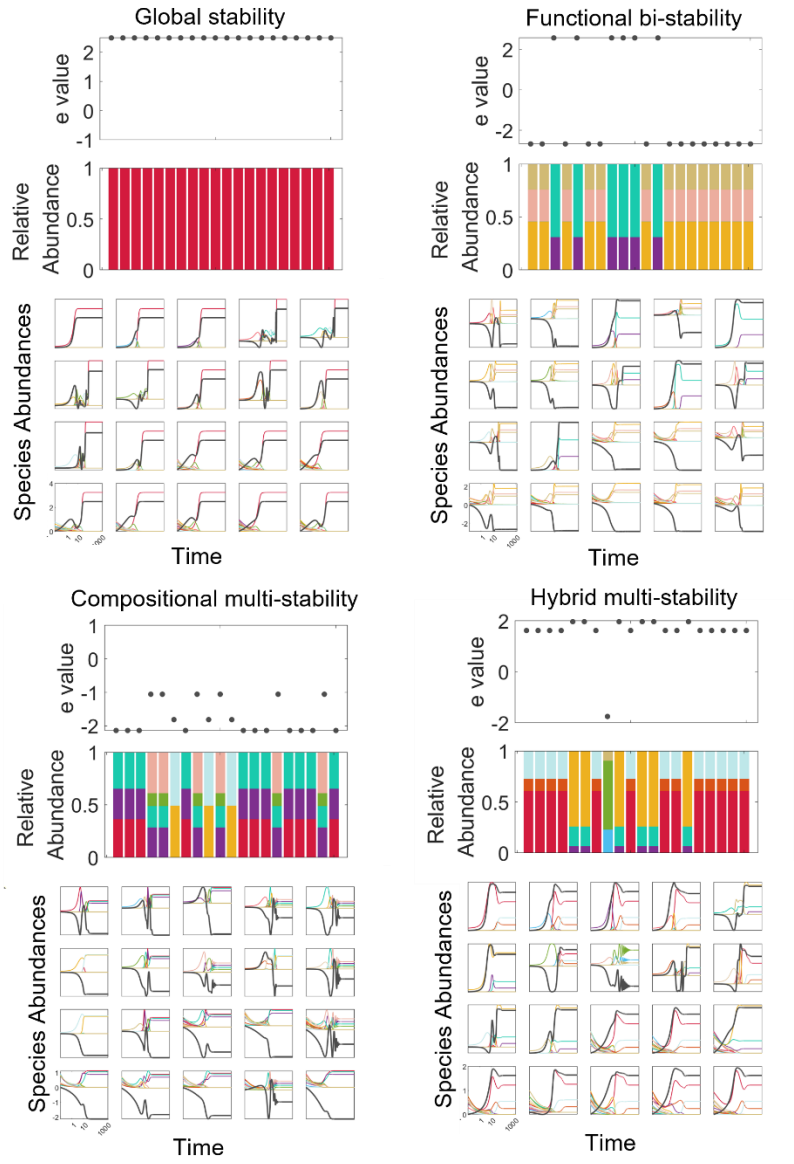

Figure S31. The eLV model recapitulated the typical outcomes in experiment. Four examples in eLV model, each representing a type of community. For each community, we tested 20 different initial species abundances, with the simulated time series shown in the bottom. The final stable states of the community can be globally stable in species abundances and e value. They can also vary significantly in e value, showing functional bistability. The community can also multiple different stable species compositions but exhibit similar e value, exhibiting compositional multistability. They can also hybridize the two mechanisms, representing hybrid multistability.

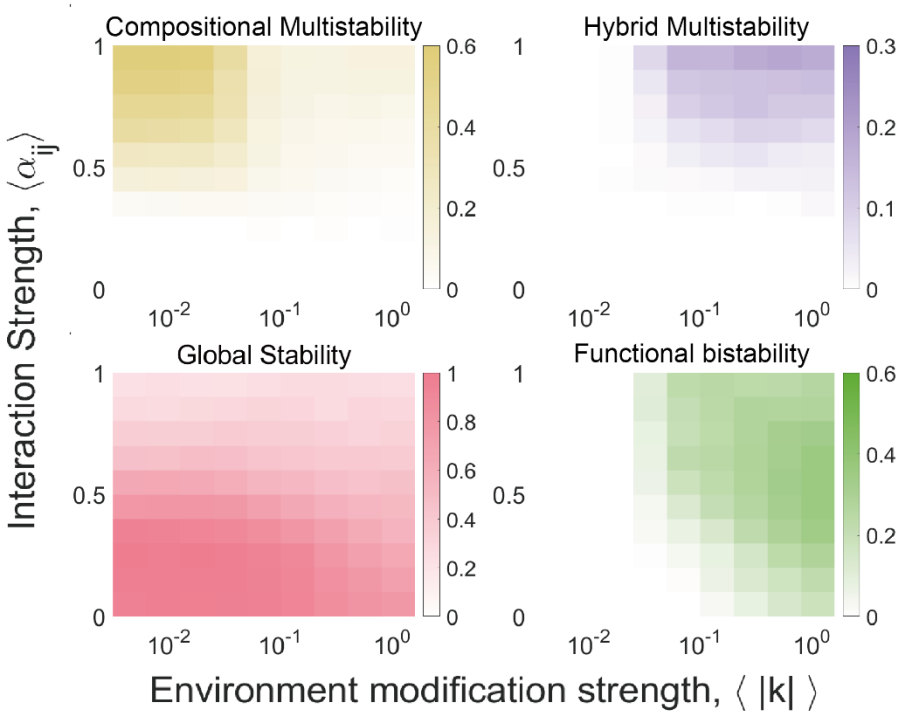

Figure S32. The eLV model predicted frequency of community types in different conditions. We varied both the species interaction strength and the environmental modification strength in the eLV model, sampling 500 communities for each parameter set. We then calculated the fraction of communities exhibiting global stability, functional bi-stability, compositional multistability, and hybrid multistability. The result shows that functional bistability arises under strong environmental modification and medium species interaction strengths, compositional multistability occurs under weak environmental modification and strong species interaction, and hybrid multistability emerges under high species interaction combined with strong environmental modification.

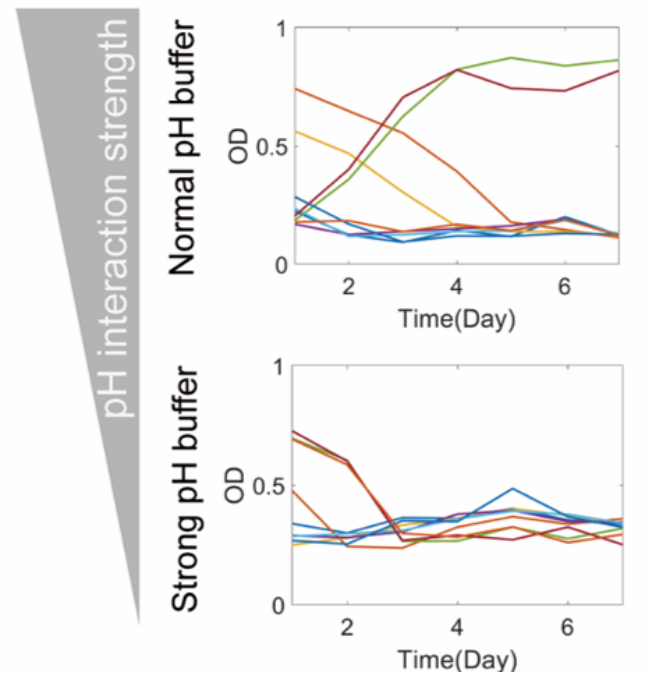

584

585 **Figure S33. The experiment validated the eLV prediction.** By adding a strong pH buffer, we
586 reduced the environmental modification strength (in this case, pH) and transitioned the community
587 from two functional regimes to a single regime. This observation further supports the eLV model's
588 prediction that hybrid multistability emerges under high environmental modification.

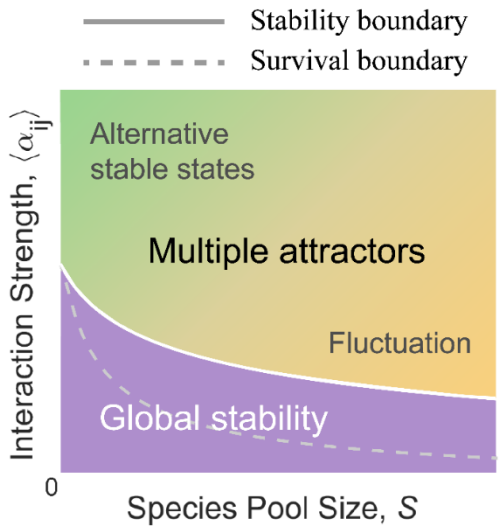

Figure S34. Cartoon phase diagram of ecological communities. Based on the gLV model and experiments, the cartoon phase diagram shows several dynamical outcomes of ecological communities. Increasing interaction strength leads to a transition from global stability to multiple attractors, which can include both alternative stable states and fluctuating attractors, depending on initial species abundances. The model predicted that, in multi-attractor phase, small species pool sizes and large interaction strengths primarily give rise to multistability with no fluctuation, while large pool sizes and medium interaction strengths tend to result in fluctuation with no stable states. Together, increasing either of the two parameters increases the fraction of communities with multiple stable and fluctuating attractors, especially at large species pool size and strong species interaction. The stability boundary and survival boundary are based on analytical results. Survival boundary separates phase I (globally stable full coexistence) and phase II (globally stable partial coexistence). Stability boundary separates phase I, II (global stability) and phase III (multiple attractors).

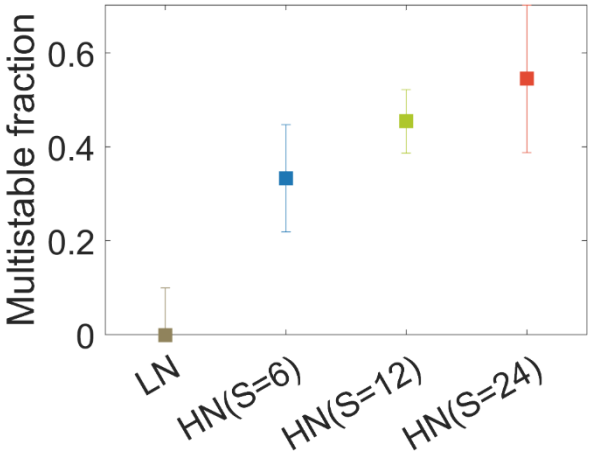

Figure S35. The relation between multistability fraction and species pool size. By calculating the multistable community fraction across different species pool sizes (S = 6, 12, and 24), we found no evidence of significant variation in multistability with increasing species richness. Pairwise two-sample t-tests revealed no statistically significant differences between groups (S=6 vs S=12: p = 0.3735; S=6 vs S=24: p = 0.2766; S=12 vs S=24: p = 0.5881), with all comparisons failing to reject the null hypothesis. These consistent results suggest that, within the tested range, the multistable fraction of communities remains unaffected by the size of the species pool, implying that other ecological factors may play more dominant roles in determining system multistability.

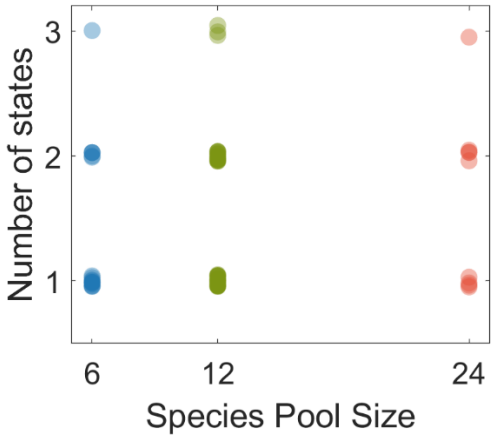

Figure S36. The relation between the number of stable states and the species pool size. We did not observe a significant increase in the number of stable states with the size of the species pool in our experiments. The correlation coefficient is 0.1142 ($p = 0.3009$).

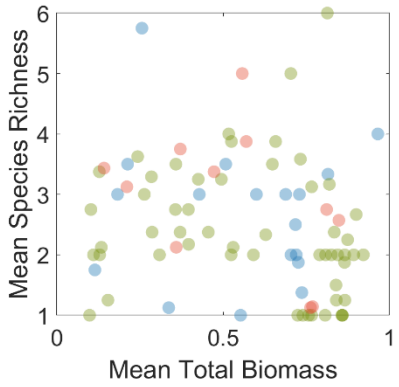

Figure S37. The correlation between diversity and total biomass in stable communities. The mean total biomass is the average community total biomass over all the replicates for a single community. The mean species richness is consistent with previous definition. We didn't observe significant correlation between diversity and biomass within the identified stable states in our experiments (corrcoef = -0.1966, p = 0.0731).

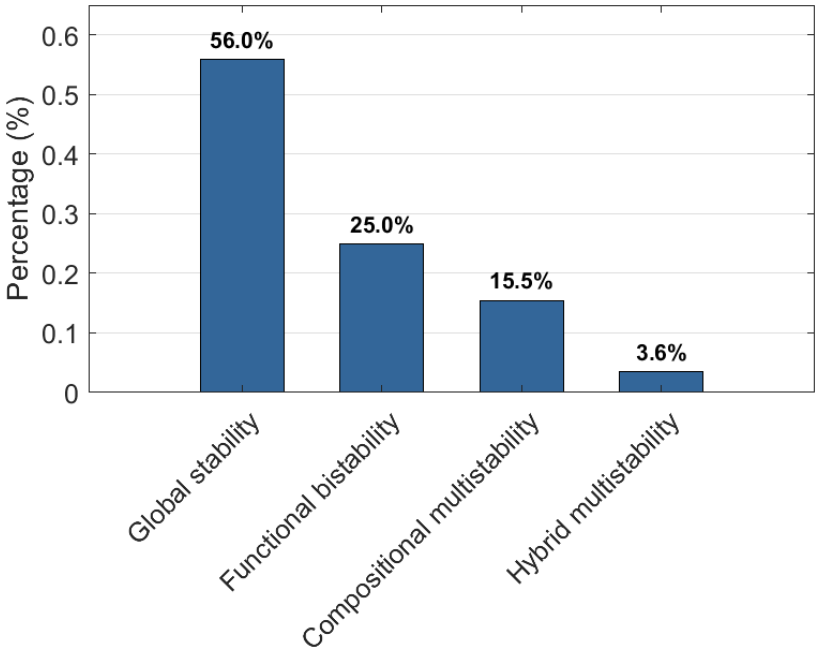

Figure S38. Fraction of four types of stable communities. Based on the classification in the main text (Figure 4), the fractions of four types of communities are calculated. In particular, the fraction of hybrid multi-stable communities is relatively low (3.6%), approximately equal to and slightly lower than the probability if the two mechanism (pH-driven functional bistability and complex network driven compositional multistability) work independently (25.0% * 15.5% = 3.9 %).